

loaded from AVISO (<https://www.aviso.altimetry.fr/en/data/products.html>).

Maps of Sea Surface Temperature (SST) were obtained from Operational Sea Surface Temperature and Sea Ice Analysis (OSTIA) database (http://ghrsst-pp.metoffice.com/pages/latest_analysis/ostia.html), which supplies 5 km resolution images of SST. Sea Surface Salinity (SSS) was obtained from Soil Moisture Active Passive (SMAPV2) dataset (https://podaac.jpl.nasa.gov/dataset/SMAP_RSS_L2_SSS_V2?ids=Collections&values=SMAP-SSS). Daily river discharge data for the La Plata estuary was obtained from the Argentinean Hydrologic Agency (Borús et al., 2008).

As shown in section 1.2.2.1, the behavior of normally incident internal waves approaching abrupt topography can be predicted from α ,

$$\alpha = \frac{\partial H / \partial x}{\gamma}, \quad (2.12)$$

where $\partial H / \partial x$ is the topographic slope and $\gamma = \tan \theta = [(\omega^2 - f^2) / (N^2 - \omega^2)]^{1/2}$ is the internal wave characteristic slope. N^2 was calculated from climatological annual mean averages of temperature and salinity for the region, obtained from the World Ocean Atlas (WOA) database.

The SML is the quasi homogeneous layer in the upper ocean where variation of density is negligible, whose depth was calculated from the TS profiles and a temperature difference criterion of 0.2° (e.g., Thomson and Fine, 2003; De Boyer Montégut et al., 2004).

Chapter 3

Results

3.1 Part I: buoyancy-driven effects on turbulent diffusivity induced by a river plume in the SBS

3.1.1 Field observations

3.1.1.1 Hydrographic observations: first cruise (early June of 2015)

High resolution transects of salinity (Fig. 3.1, panel (a)) and temperature (panel (b)) highlight the variability associated with the presence of the plume. PPW is observed at the surface along the entire transect, reaching the vicinities of the shelf break. Our observations show that the plume interface follows along the $\sim 23.5 \text{ kgm}^{-3}$ isopycnal. The liftoff point of the plume, i.e., the location where the bottom attached salinity front loses contact with the bottom, is visible at the inner shelf region, approximately 50 m depth and 35 km from the starting position of the transect (about 75 km from the coast). TW and SACW are also observed in the final portion of the transect, as it reaches the shelf break. Warm and salty TW is associated with the southward flow of the Brazil Current (Soares and Möller, 2001) and SACW is ubiquitous on the Brazilian continental shelf from the northern portions of the South Brazilian Bight (e.g., Castro, 2014; Cerda and Castro, 2014) to the Brazil-Malvinas Confluence (e.g., Piola et al., 1999; Möller et al., 2008). Colder waters from the SACW may intrude the shelf region because of instabilities associated with the meandering of the Brazil Current as it flows along the shelf-break (Lima et al., 1996). Along the boundary between PPW and TW, STSW is observed, formed due to mixing between those water masses.

The transect of buoyancy frequency (Fig. 3.2, panel (a)) shows the strong stratification induced by the plume in this portion of the SBS. Values up to 0.05 s^{-1} , in the mid-section at the continental shelf, and close to the surface at the shelf break, are observed. The vertical shear of the horizontal, geostrophic velocities (panel (b)) is mostly weak along the transect, but it is enhanced at the shelf break close to the surface, sug-

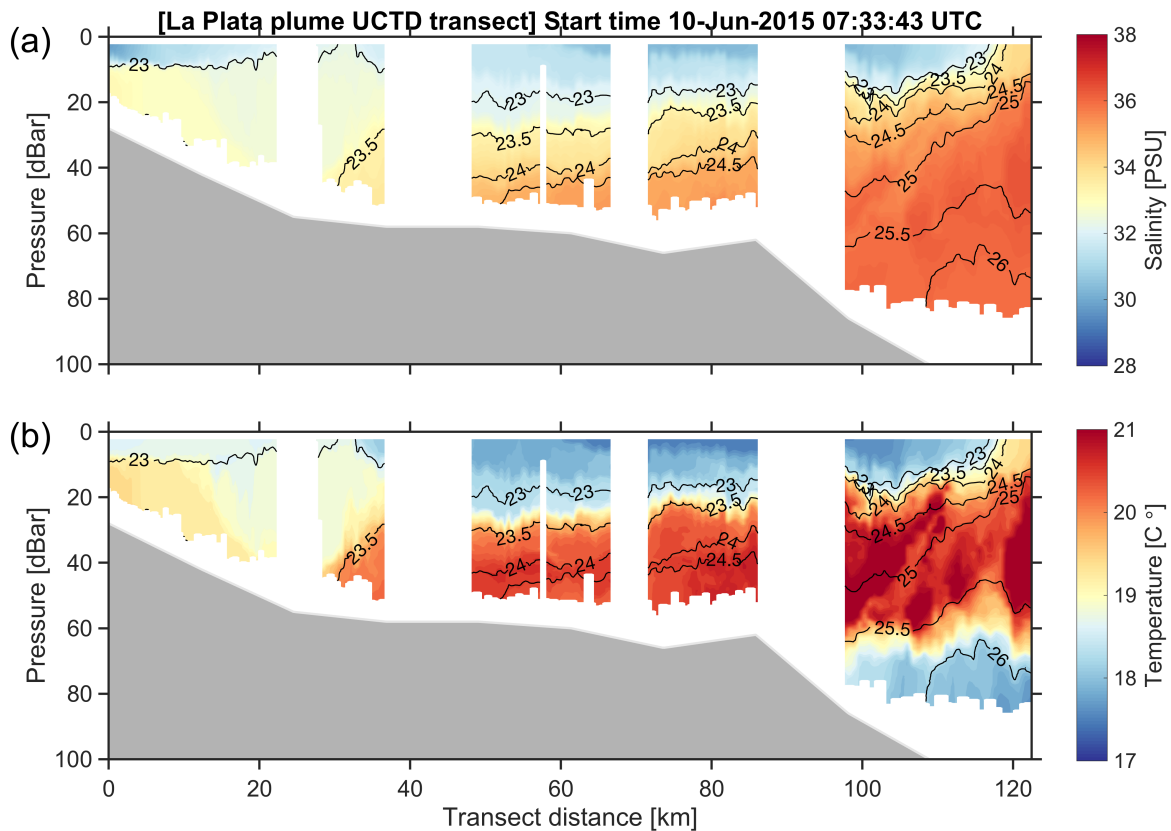


Fig. 3.1: High resolution hydrographic transects of (a) salinity and (b) temperature obtained with the UCTD. The black lines are the isopycnals in kgm^{-3} .

gesting strong advection (northward at the southern hemisphere) at the most offshore portion of the transect. This strong shear led to the reduction of Ri_g at this location (panel (c)). Low values are observed from the surface to the bottom of the profiles, suggesting that instabilities are occurring at the shelf break. This is consistent with what appears to be a vertical intrusion observed at, approximately, 50 m depth, which is clearer on the temperature data (c.f., Fig. 3.1, panel (b)). Warm and saltier water on the shallow side rises while fresh and colder water on the deeper side of the shelf sinks, suggesting a vertical overturning at a sloping bottom, followed by a geostrophic jet (e.g., Wang, 1984). Over continental shelf, Ri_g increases substantially in the mid transect section, where layers of enhanced N are observed, suggesting strong stability. Low values of gradient Richardson number are also found at the shallow inner shelf portion, where stratification is weakened due to the shallow depth.

3.1.1.2 Microstructure observations: second cruise (early July of 2015)

For effects of comparison between cruises, the La Plata River daily discharge (Fig. 3.3) shows no significant changes from the first to the second cruise, varying between $\sim 21000\text{-}25000 \text{ m}^3\text{s}^{-1}$. The same happened for the SST distribution (Fig. 3.4), where

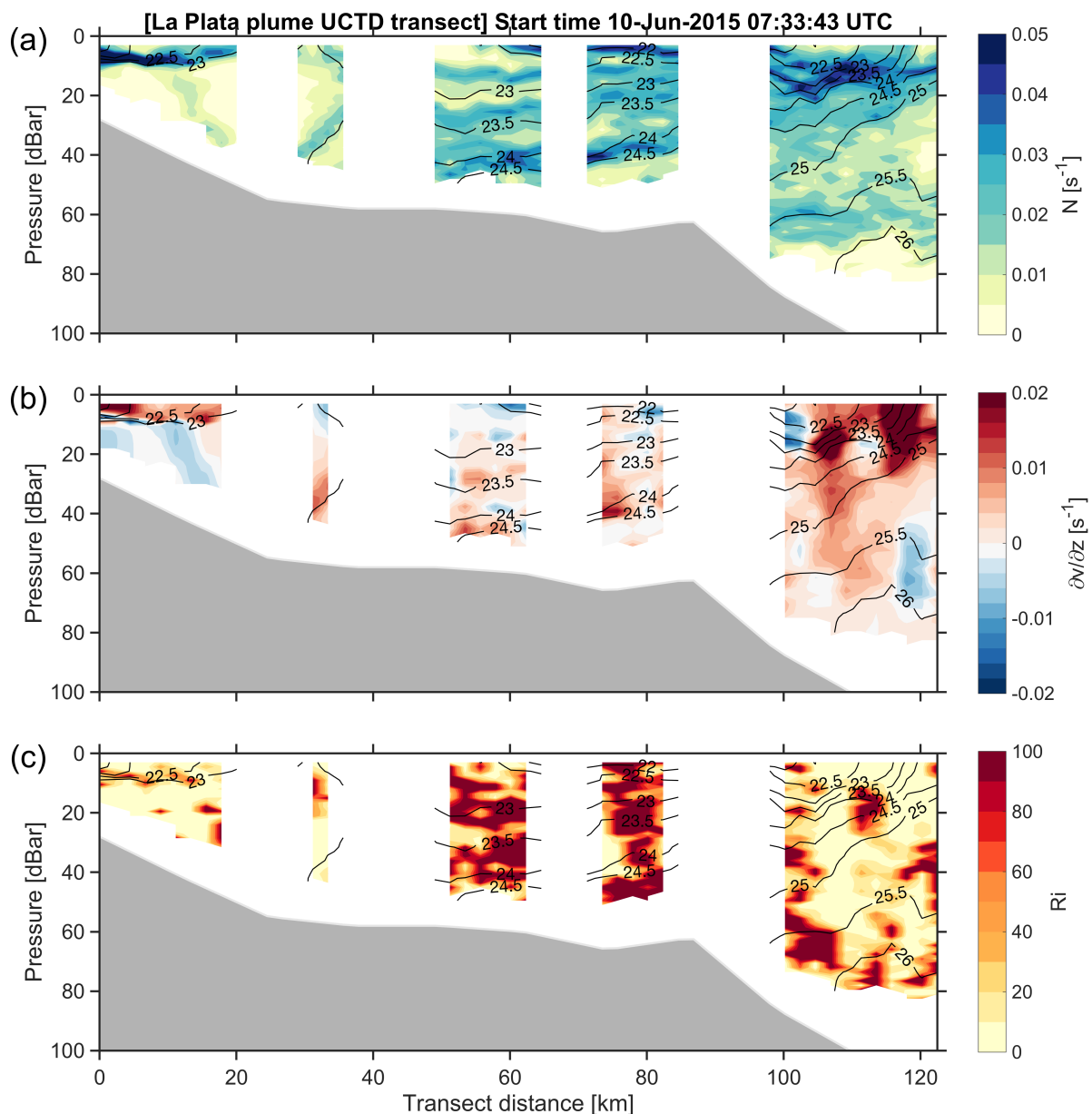


Fig. 3.2: Transects of (a) N , (b) $\partial v / \partial z$ and (c) Ri_g estimated with UCTD data. The black lines are the isopycnals in kgm^{-3} .

the plume did not alter significantly its temperature or position during the time apart between cruises.

In Fig. 3.5 and 3.6, are hourly time series of net heat flux (panel (a)) and wind shear (panel (b)) for the location of each transect of VMP-250 profiles. The weather conditions were more or less stable during most of the second cruise. However, in July 3 the passage of a frontal system caused a large increase in the surface wind shear and surface heat loss during the time of the last stations of the AL transect. These frontal systems are very common in the subtropical southwestern Atlantic, specially during Austral winter (Stech and Lorenzetti, 1992). Wind shear was significantly reduced at

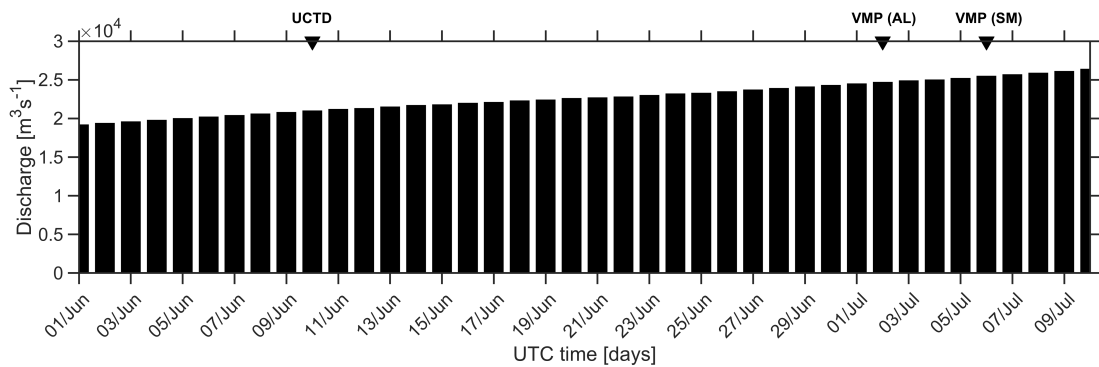


Fig. 3.3: Daily river discharge from La Plata River measured by the Instituto Nacional del Agua (Ezeiza, Argentina - 2008). The black triangles are the times of the UCTD and the VMP-250 transects.

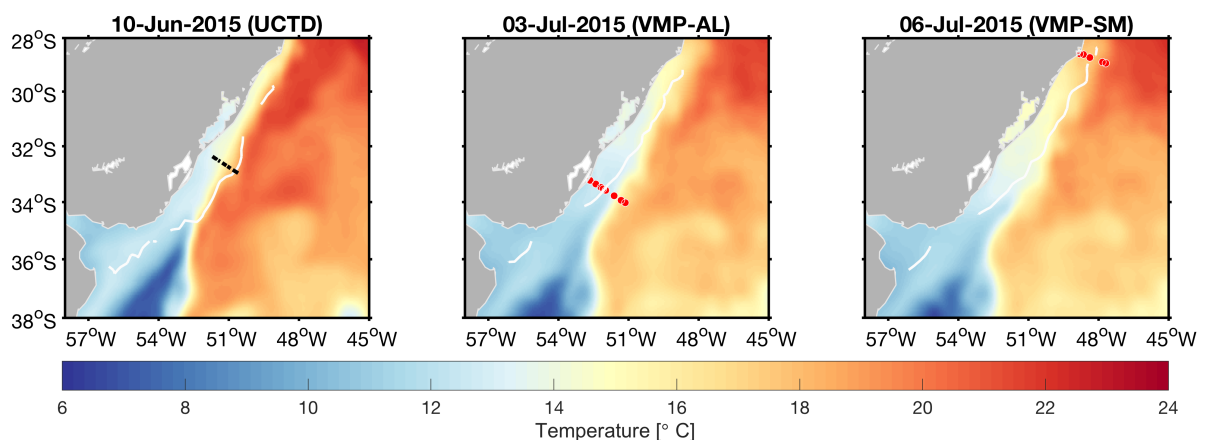


Fig. 3.4: 5 km resolution Sea Surface Temperature (SST) daily images from OSTIA data base. The panels refer to UCTD transect (left), VMP AL transect (middle) and VMP SM transect (right). The black lines are is UCTD transect, the red dots the VMP stations and the white line is the 33.5 PSU isohaline.

the SM transect location, yielding no significant influence on surface mixing.

The frequency of occurrence of K_T and R_ρ for both transects were clustered into continental shelf and shelf break data due to differences regarding the presence of PPW. For the AL transect, K_T was nearly normally distributed (Fig. 3.7, panel (a)), being similar for continental shelf and shelf break. A storm occurred at the end of the AL transect, which enhanced mixing and surface K_T in the shelf break profiles, increasing the occurrence of larger values. The averages of each distribution were similar, being slightly larger at shelf break. For the SM transect (Fig. 3.8 panel (a)), on the other hand, the distributions were unequal for both areas, being nearly bi-modal. This happened because of the smaller amount of plume waters in the continental shelf off Sta. Marta Cape, allowing increased levels of vertical diffusivity in the shelf region, on average, nearly one order of magnitude greater than at the shelf break.

The R_ρ distributions (panel (b) in Fig. 3.7 and Fig. 3.8) evidence the differences between continental shelf and shelf break. In the shelf break profiles, DDC can be developed by salt-fingers, where warmer and saltier TW lies over colder and fresher SACW. In the continental shelf, conversely, where colder and fresher waters from the

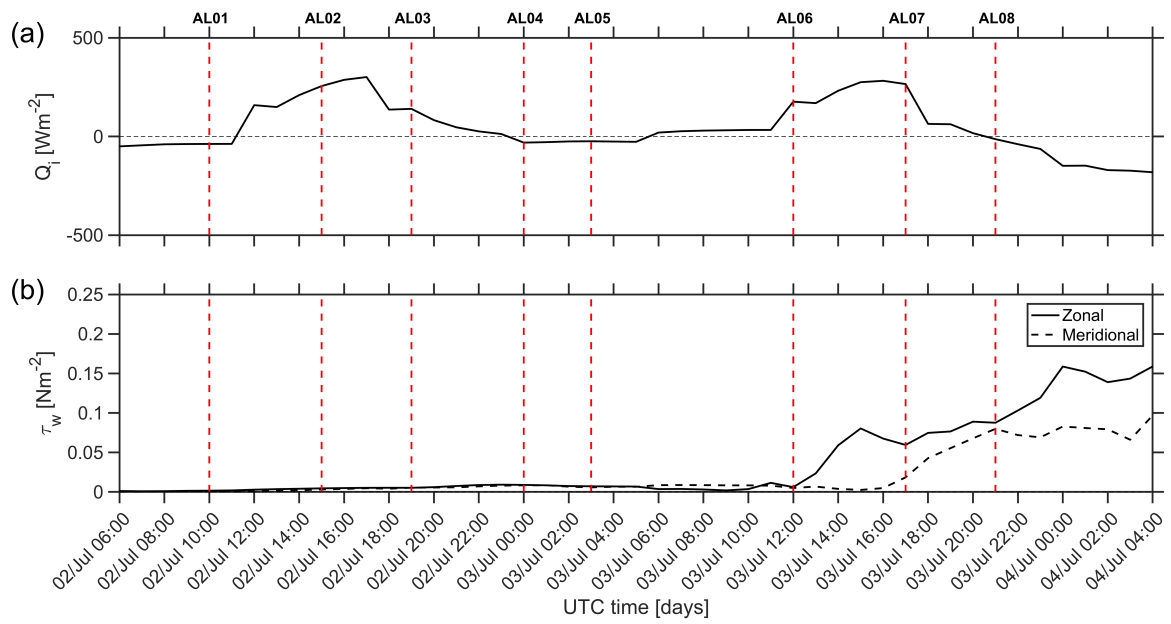


Fig. 3.5: Spatially averaged hourly time series of (a) net heat flux and (b) wind shear for the location of the **AL** transect. The red dashed lines is the time of each station.

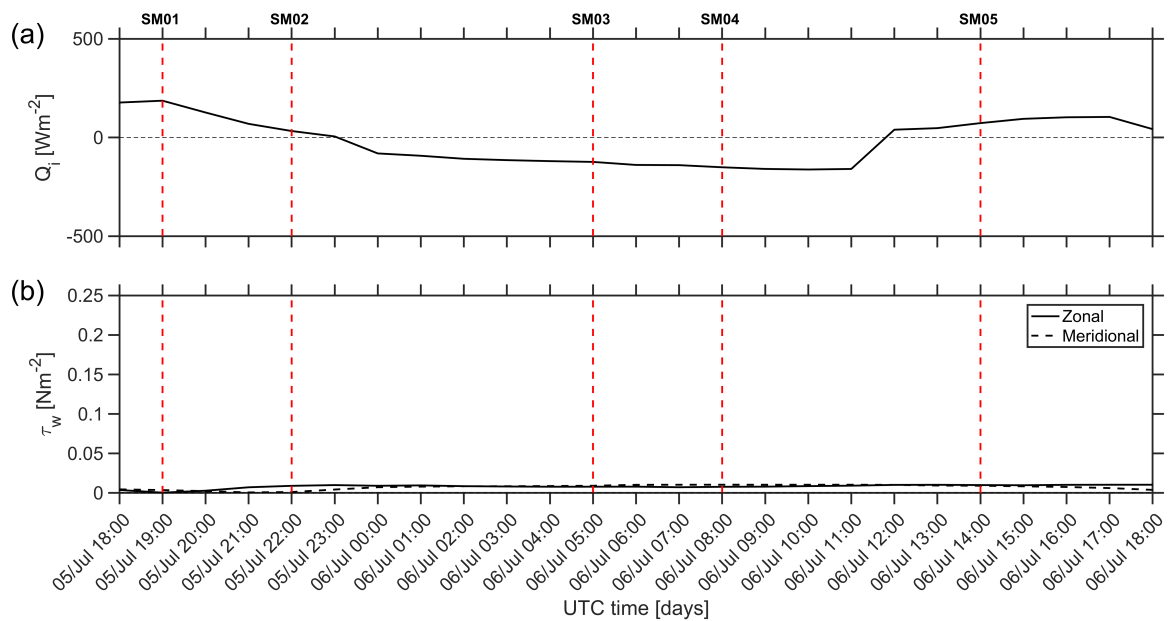


Fig. 3.6: Same of Fig. 3.5 for the **SM** transect.

plume stand above relatively warm and salty oceanic waters, DDC can occurs due to a diffusive regime. Actually, the distribution mode of R_ρ in the continental shelf for the AL transect suggests that diffusion is unlikely to occur since the most frequent values were around 0.01. This is result of the strong stratification induced by plume waters in the southern portion of the SBS. For comparison, in the SM transect the mode is around 0.28, which is more likely to yield diffusivity.

The profiles of N in the AL transect (Fig. 3.9, panel (a)) match the hydrographic observations from the UCTD, with values up to 0.05 s^{-1} at the plume interface, the well

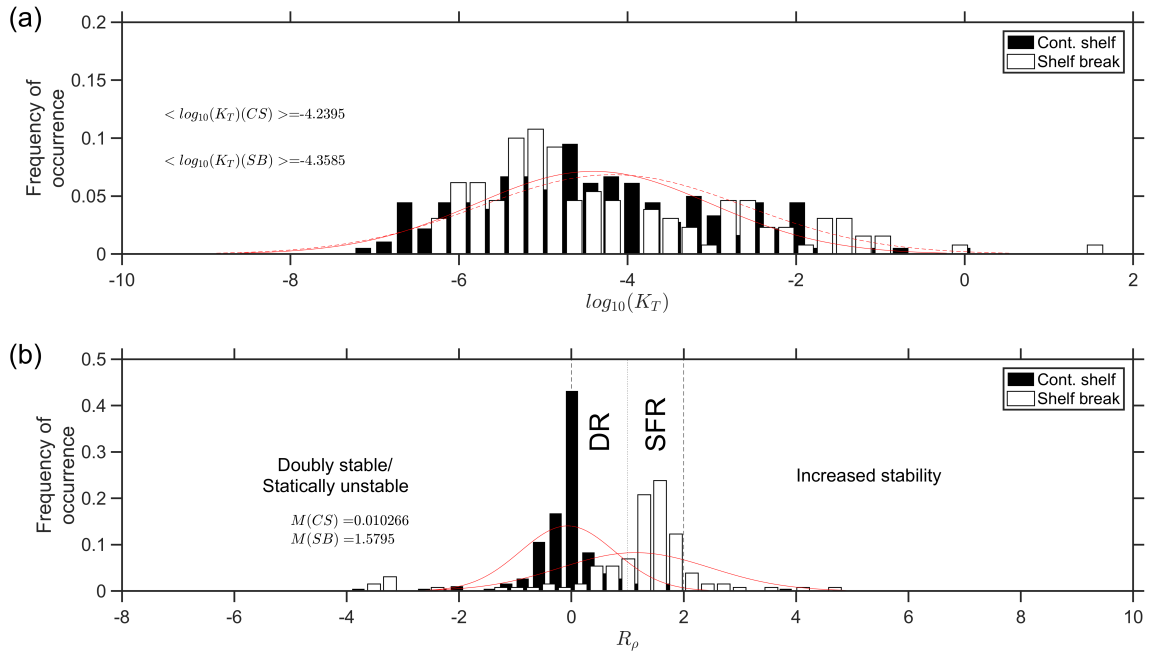


Fig. 3.7: Frequency of occurrence of K_T and R_ρ for the **AL** profiles. In panel (b), DR stands for diffusive regime and SFR for salt-finger regime. The vertical dashed lines in (c) refer to the thresholds within each type of DDC regime is prone to occur. The red lines are the log-normal probability functions fitted to the data (full for continental shelf, dashed for shelf break). The ensemble average of each distribution is displayed in the figures.

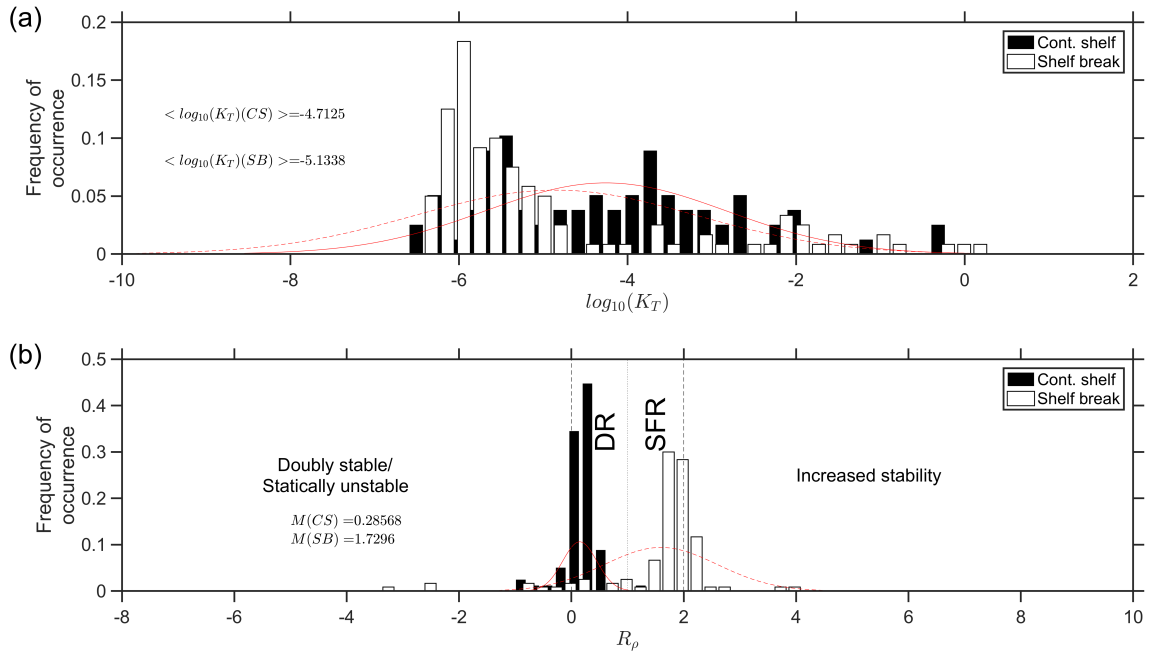


Fig. 3.8: Same of Fig 3.7 for the **SM** profiles.

stratified layer from stations AL03 to AL06, around 25 m depth. Below the $\sim 25 \text{ kg m}^{-3}$ isopycnal stratification is considerably reduced and the surface mixed layer (SML) sinks significantly beyond the shelf break. This significant sinking of the SML depth is also related to a storm that occurred near the location of station AL08. The strong vertical

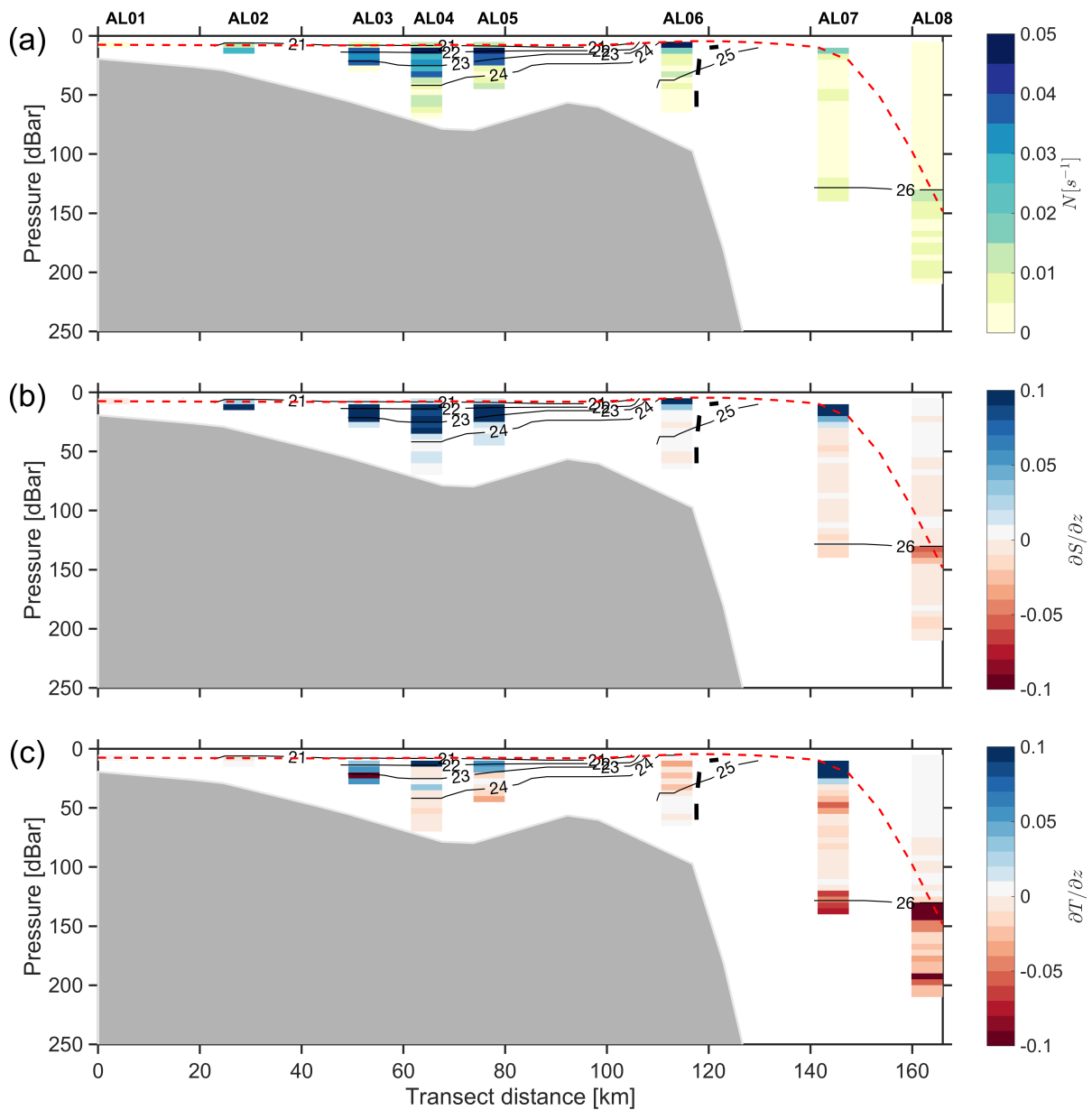


Fig. 3.9: Vertical profiles of (a) N , (b) $\partial S/\partial z$ and (c) $\partial T/\partial z$ calculated from microstructure data for the **AL** transect. The black lines are the isopycnals in kgm^{-3} , the thick dashed black line is the 33.5 PSU isohaline and the red dashed line is the SML depth.

shear induced by this event caused the SML to reach nearly 135 m depth at this station. At the location of the SM transect, a substantial reduction in N occurs (Fig. 3.10, panel (a)) and a retreat of the plume interface towards the coast is observed.

Salinity and temperature gradients for both transects (Fig. 3.9 and 3.10, panels (b) and (c)) highlight the freshwaters over the continental shelf, as well as the stronger gradients in the southern transect, specially of salinity. Because of the buoyancy-driven salinity, temperature increases with depth (within the plume layer), an ubiquitous feature for all locations where PPW is observed (e.g., Castello and Möller, 1977).

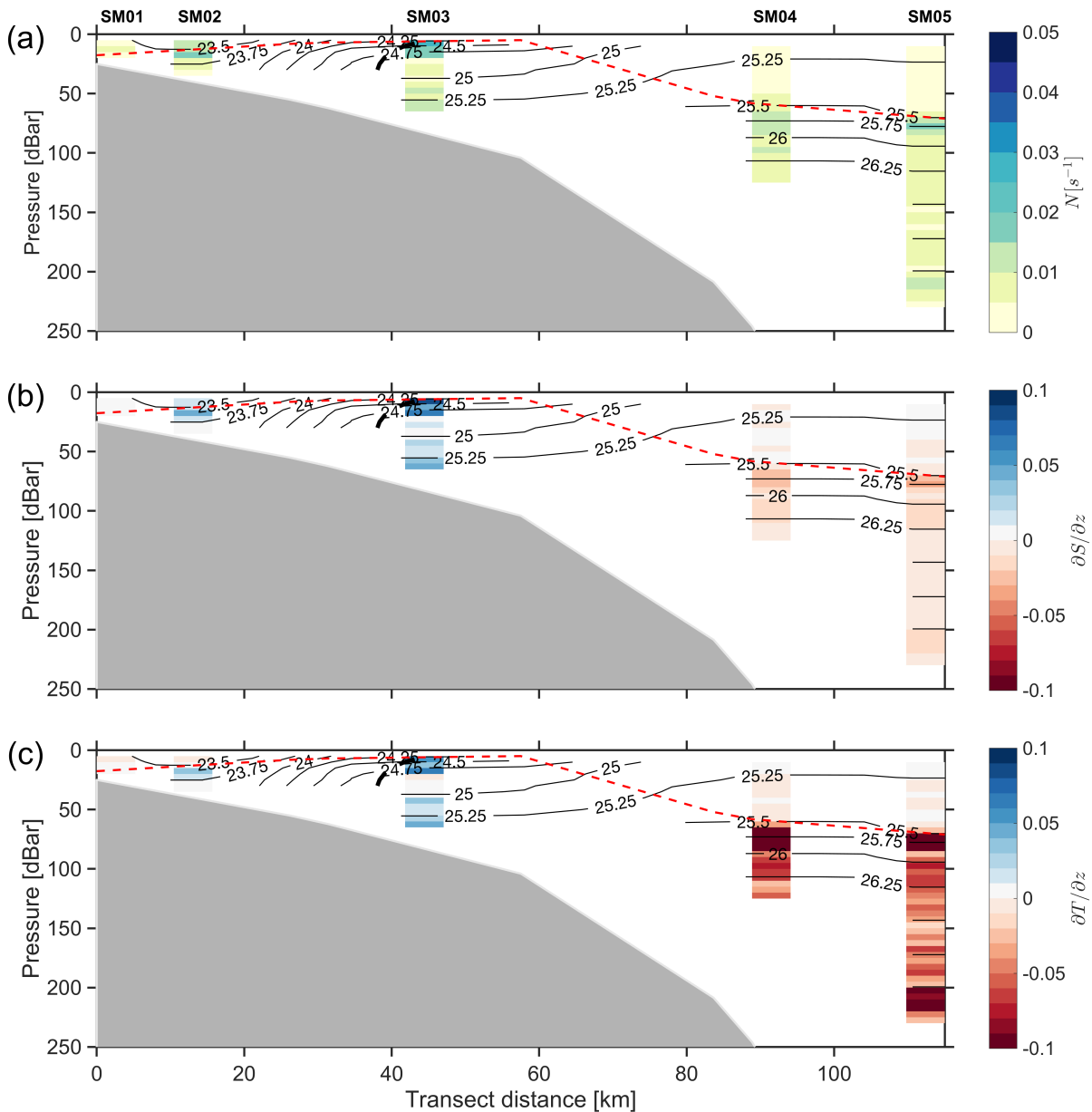


Fig. 3.10: Same of Fig. 3.9 for the **SM** transect.

In the AL transect, K_T and B_f (Fig. 3.11, panels (a) and (b)) are significantly increased within the SML at AL08. In fact, heat diffusivity is very large, up to $\mathcal{O}(-2)$ m^2s^{-1} . Both heat diffusivity and buoyancy flux are reduced towards the continental shelf, mainly at the plume interface. At this location a reduction of nearly four orders of magnitude, when compared to the SML in AL08, is observed. In the SM transect, K_T and B_f are also large in the SML at the shelf break profiles (Fig. 3.12, panels (a) and (b)). But since no strong mixing event occurred, these relatively large values may be associated with surface convection, as the SML depth is nearly the same for both profiles, around 75 m. Heat diffusivity and buoyancy flux are reduced in the continental shelf, but not as much as observed in the AL transect. In fact, at the plume interface,

no clear reduction in diffusivity is observed, as stratification is not as strong as in the location of the AL transect.

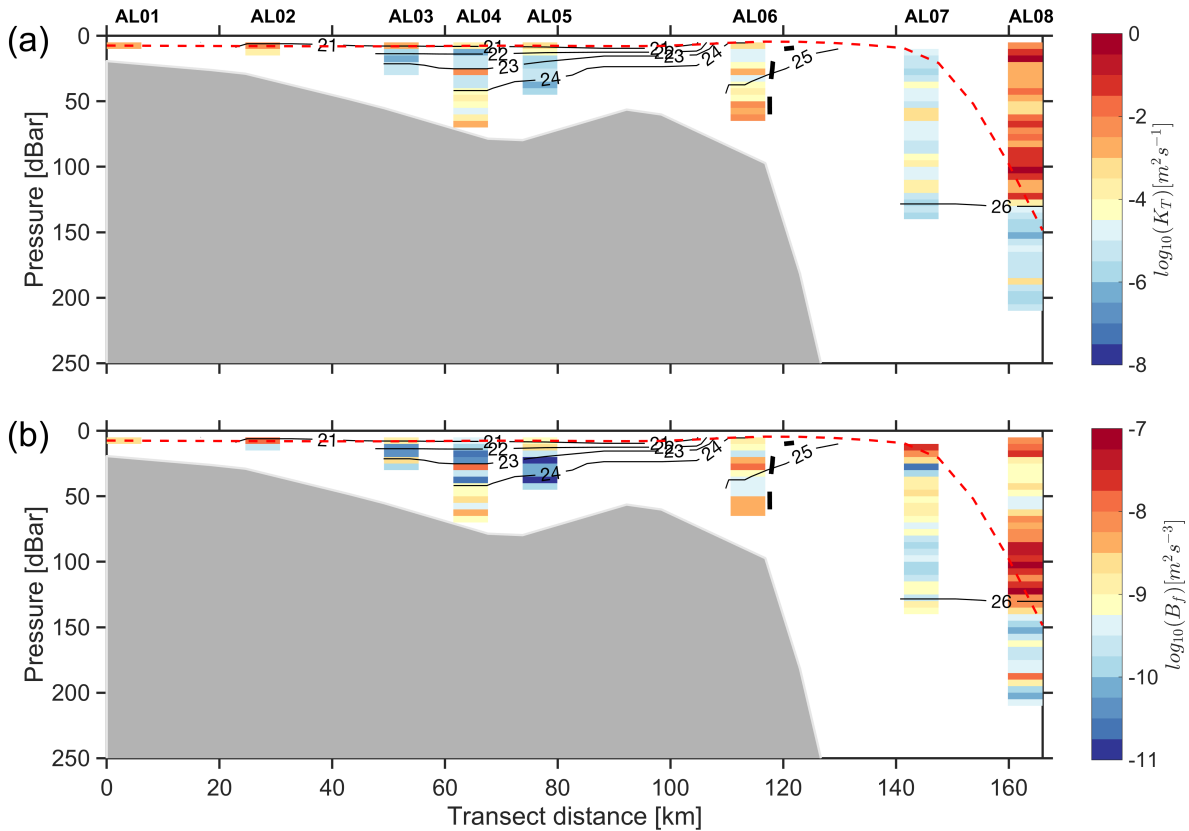


Fig. 3.11: \log_{10} profiles of (a) K_T and (b) B_f for the **AL** transect. The black lines are the isopycnals in kgm^{-3} , the thick dashed black line is the plume boundary and the red dashed line is the SML depth.

3.1.1.3 Individual profiles (AL04, AL08, SM05 and SM03)

These four profiles were selected to demonstrate the dynamical differences found in the SBS. AL08 and SM05 were made at the shelf breaks areas of Albardão and Sta. Marta Cape, while AL04 and SM03 were taken in areas influenced by plume waters.

- Profile **AL04** (Fig. 3.13): At the location of this profile, strong stratification is observed, where N peaks $\sim 0.07 \text{ s}^{-1}$ at approximately 10 m depth. As both temperature and salinity increase with depth, DR may be developed. However, there is no sign of well developed thermohaline staircases, A SML is visible on the first 10 m, where L_T , K_T and B_f are increased. Below this depth, however, all three are significant reduced due to stratification. The lack of shear-stratified flows is evidenced when comparing the profiles of N and L_T . The product $L_T N$ may be an indicator of active shear-stratified turbulence¹. However, since the

¹A estimative of dissipation can be obtained using the relation $\epsilon = cL_T^2 N^3$. However, it depends on $c = (L_O/L_T)^2$, and a significant amount of uncertainty relies on the ratio of the Ozmidov and Thorpe scales, as they are linked to the temporal variability of turbulent overturns [Smyth and Moum (2000)]

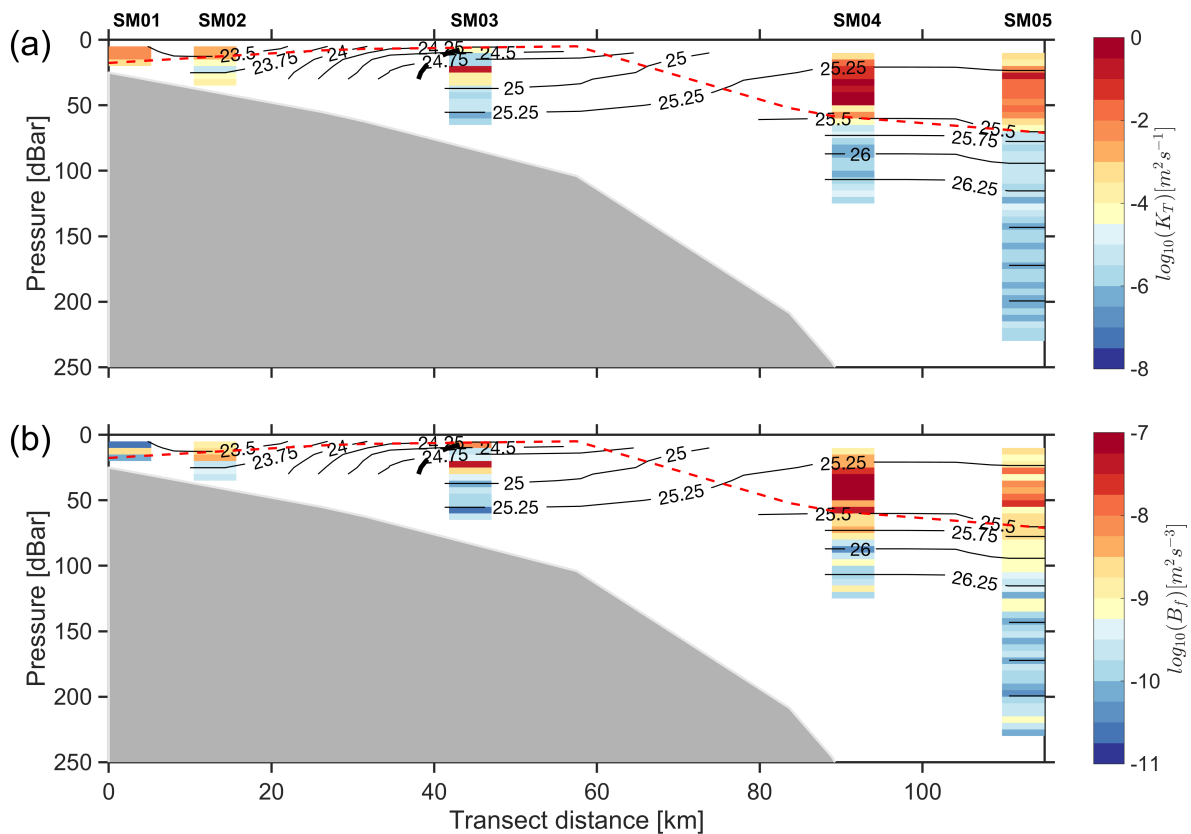


Fig. 3.12: Same of Fig. 3.11 for the **SM** transect.

profiles of N and L_T have opposite behaviors, it is unlikely that active shear is occurring.

- Profile **AL08**, (Fig. 3.14): This profile is much different than AL04, as there is no influence of freshwaters. The dynamics at AL08 is instead influenced by the strong meteorological event. The mixing caused by this event increased greatly the levels of B_f and K_T in the SML. As a consequence of the shear input, L_T is significantly enhanced at the base of the layer. The magnitude of the stratification, $\sim 0.03 \text{ s}^{-1}$, is much less when compared to the one registered at VT04. Thermohaline staircases appears to be present, where L_T is reduced, which may be an indicative of SFR. Density overturns are also enhanced at approximately 180 m, the interface with colder and fresher waters from SACW, where shear instabilities may occur, as stratification is not strong as it is at the base of the SML depth. At this layer, K_T and B_f are increased, which suggests that KH billows are transporting heat through this layer.
- Profile **SM03** (Fig. 3.15): This profile was made at the plume boundary, showing similar conditions to the AL04. However, as density gradients are reduced due to increased dilution of freshwaters with oceanic waters, stratification diminished, being $\sim 0.03 \text{ s}^{-1}$. As a consequence, L_T is slight larger in the plume interface

in comparison to AL04, as well as K_T and B_f . Staircases are barely seen, but similar structures are seen at, approximately, 15 m, where both N and L_T are increased. A DR may be occurring, but it is hard to discriminate it from heat diffusivity due to shear instabilities.

- Profile **SM01** (Fig. 3.16): Similar to AL08, this profile has no influence of freshwaters. K_T and B_f are enhanced in the SML and N is $\sim 0.01 \text{ s}^{-1}$. L_T is increased at the base of the SML due to the active mixing that increased heat diffusivity and buoyancy flux. At the bottom of the profile, at approximately 220 m, there is subtle indication of shear turbulence, as both L_T and N are increasing. This portion may be the interface with SACW, as both salinity and temperature decrease.

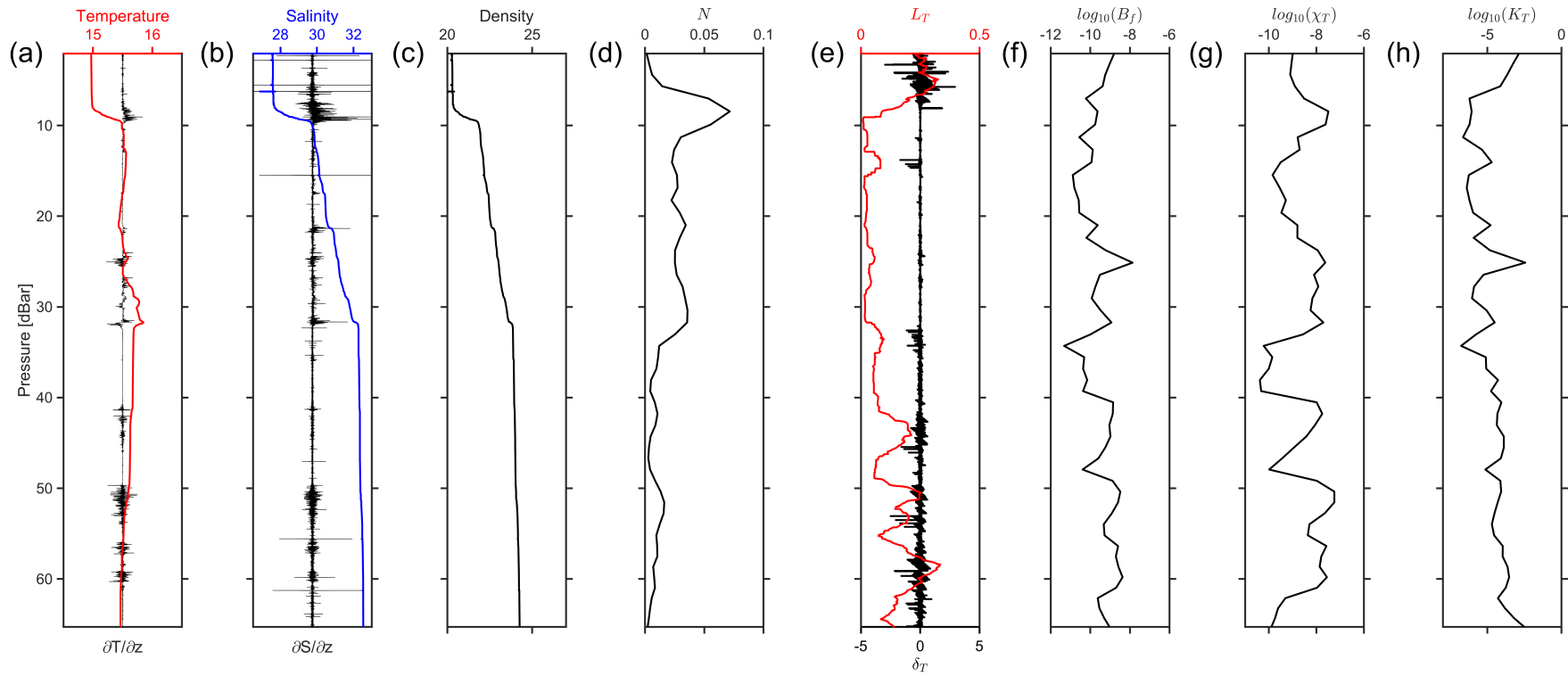


Fig. 3.13: Details from profile made at station **AL04**. In (a) temperature profile (red line) with temperature gradient (black line), (b) salinity profile (blue line) with salinity gradient (black line), (c) density, (d) N , (e) L_T (red line) and δ_T (black line), (f) $\log_{10}(B_f)$, (g) $\log_{10}(\chi_T)$ (red line) and $\log_{10}(\chi_S)$ (blue line) and (h) $\log_{10}(K_T)$ (red line) and $\log_{10}(K_S)$ (blue line).

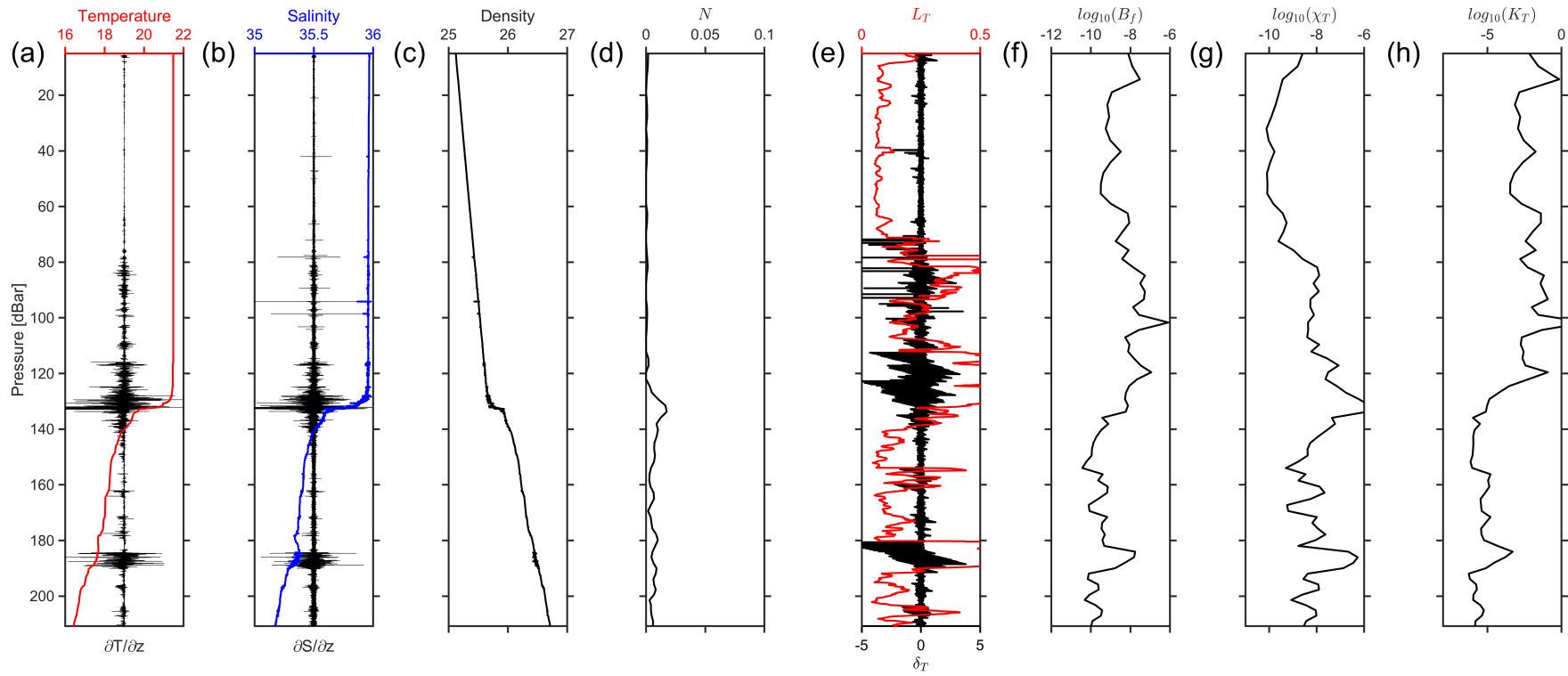


Fig. 3.14: Same of Fig. 3.13 for AL08.

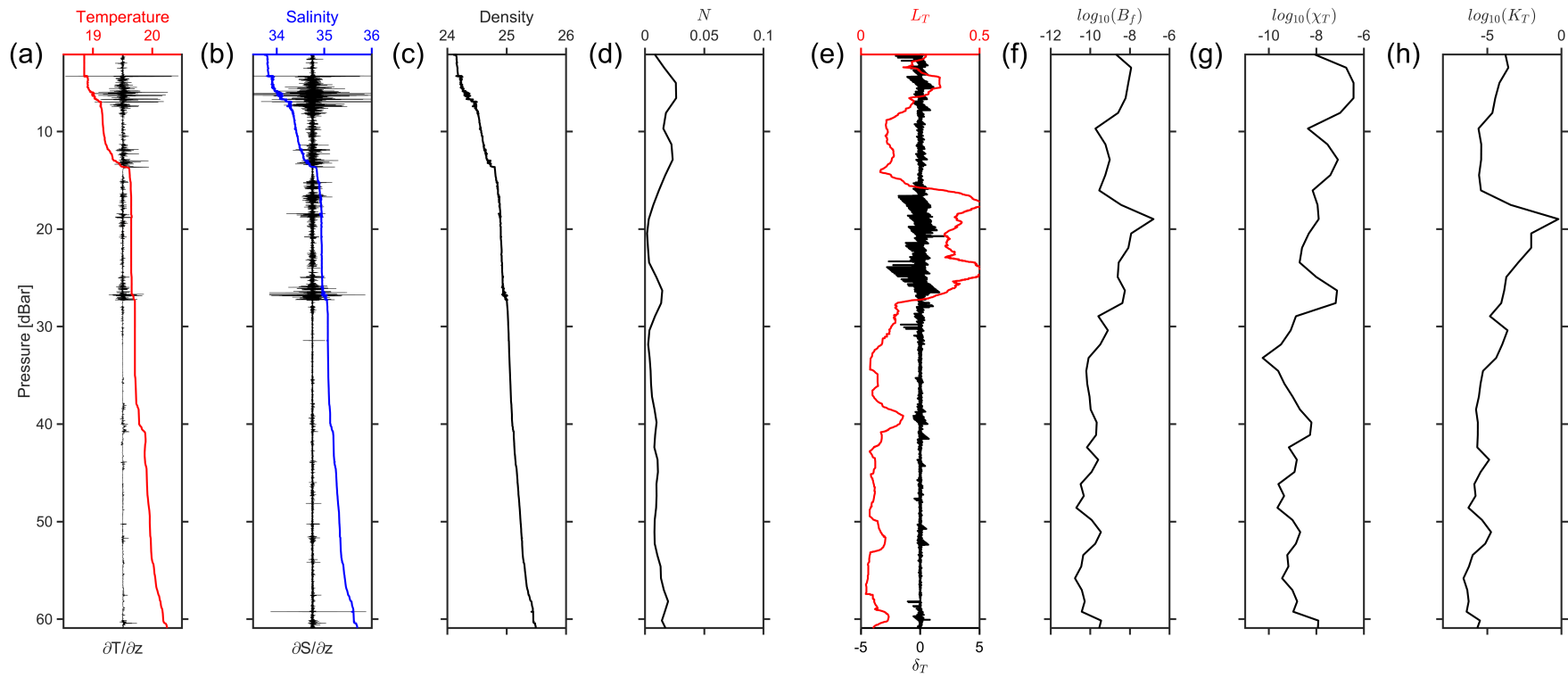


Fig. 3.15: Same of Fig. 3.13 for SM03.

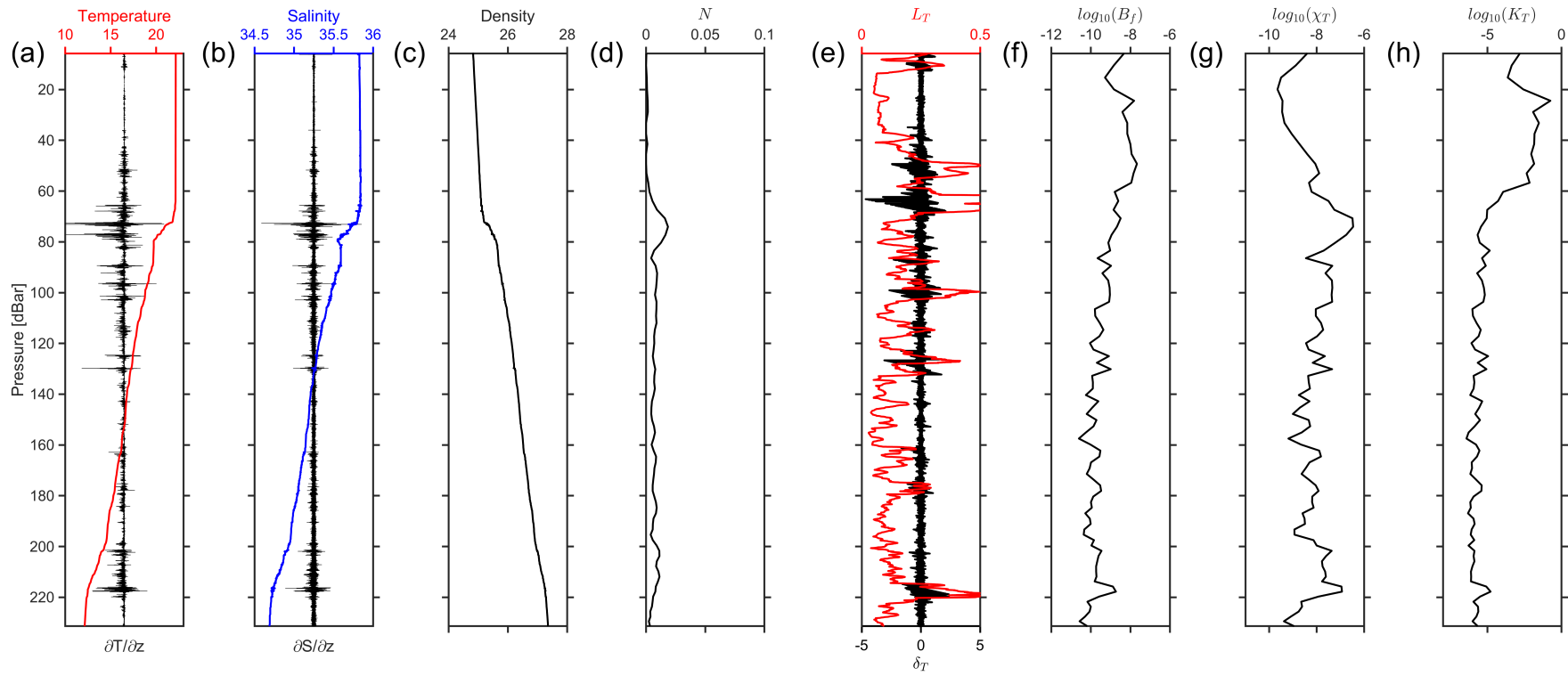


Fig. 3.16: Same of Fig. 3.13 for SM05.

3.1.2 Effects of freshwaters stratification on mixing

In general, turbulent mixing in freshwater plumes is driven by shear-stratified flow instabilities in the form of KH billows within the stratified interface (Stacey et al., 1999). The stratification induced by PPW and the high Ri_g values found on the UCTD data at the southern inner shelf implies low shear variance. Hence, the large-scale La Plata River plume reduces the level of mixing expected for a shallow continental shelf. In large-scale ROFI (Regions Of Freshwater Influence) systems, the spreading outflow tends to stratify the water column, opposed by stirring due to tides, waves and winds (Simpson, 1997). This highly stable outflow inhibits the mixing at the interface due to the positive buoyancy input from low salinity waters, which exceeds the buoyancy loss from surface cooling. In the case of La Plata River plume, the induced buoyancy is very strong, so this ROFI system remains stratified even when the other portions of the shelf are mixed. Atmospheric forcing in the SBS, specially in the southern area, is restricted to the surface due to the effective isolation from bottom layers promoted by the freshwater-driven stratification (Zavialov et al., 2002). This explains the very shallow SML depth observed within the plume and the magnitude of N observed in the plume interface.

Figure 3.17 shows δ_T calculated from the microstructure density profiles made on the SBS. Displacements are reduced in the AL profiles, more specifically, at the corresponding location of the plume interface. The density range of $\sim 21\text{-}24 \text{ kgm}^{-3}$, where buoyancy frequency reaches values up to 0.05 s^{-1} , is a strong and stable interface that inhibits mixing on the continental shelf and prevents the generation of shear instabilities. At the location of the SM transect, the density front is weakened due to higher dilution with oceanic waters. Consequently, it is more susceptible to shear-stratified turbulence, as seen by the increase in δ_T . The presence of density overturns in strongly stratified flows is an indication of the amount of TKE within a flow, rather than its rate of dissipation (Mater et al., 2013). The reduced overturns at the plume interface in the AL region suggests that the flow, although energetic as an estuarine outflow, is stable.

Near-field river plumes are usually characterized by large turbulence and mixing, commonly found at estuaries with narrow channels (e.g., Luketina and Imberger, 1989; MacDonald et al., 2007, 2013). The wide the La Plata estuary, however, will rarely generate large velocity differences between upper and lower layers and shoaling as the plume leaves the estuary. As a consequence, a near-field region will not exist in the La Plata River plume and no large turbulence is expected to occur near the source region. Due to its large spatial scale, which is larger than the internal Rossby radius (Pimenta et al., 2005), the La Plata River plume behaves as a far-field river plume, where motions are mainly driven by the Coriolis force and the wind shear away from the source region. When winds and local currents are not sufficient to advect the plume

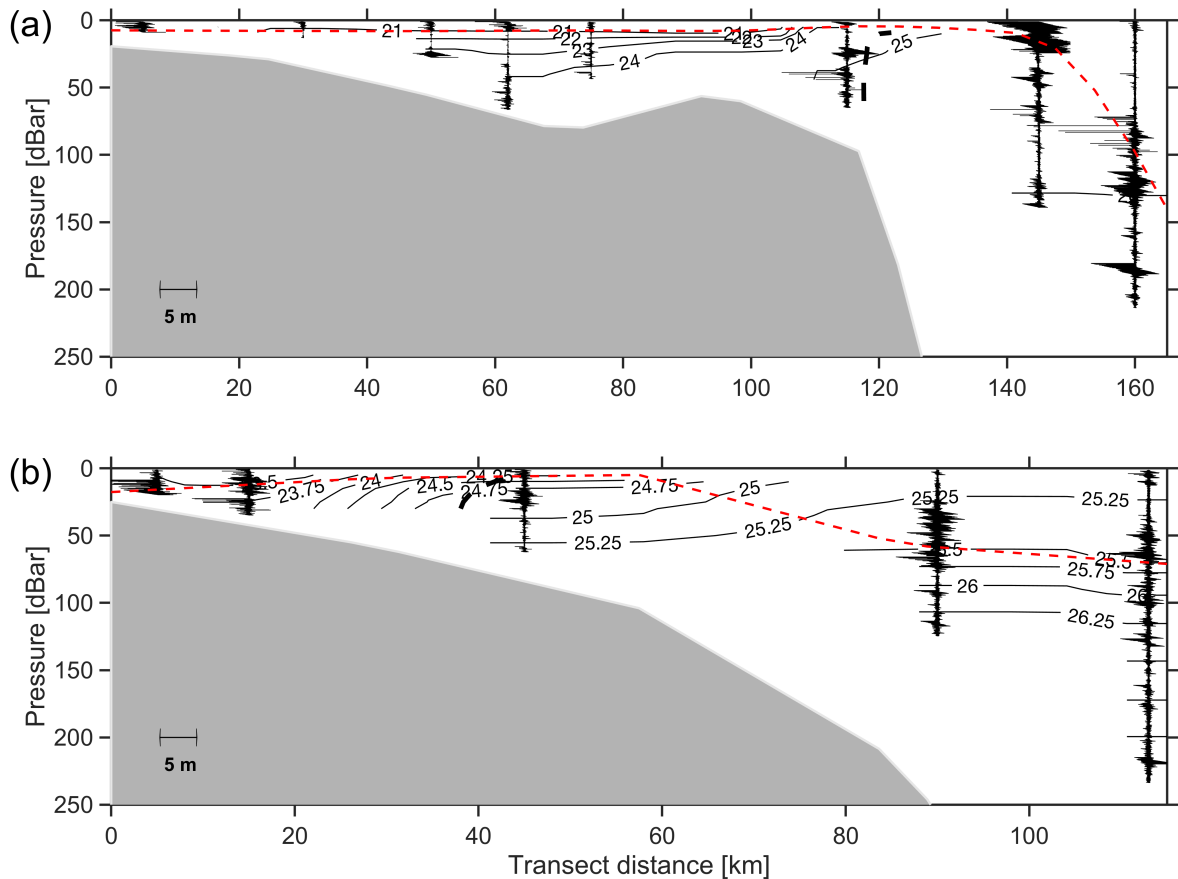


Fig. 3.17: Density displacements calculated from the observed instantaneous micro-scale density profiles from the VMP-250 for the AL (a) and SM (b) transects; the black lines are the isopycnals in kgm^{-3} ; The thick dashed black line is the plume salinity boundary; the red dashed line is the SML depth.

offshore, the far-field plume forms a geostrophic coastal current that propagates as a coastal Kelvin wave (Horner-Devine et al., 2015), leaving the coast to the left in the southern hemisphere. This northward flow of the La Plata River plume is known as the BCC (De Souza and Robinson, 2004), stronger during a SW wind regime. Although the UCTD data suggests a strong stability on the continental shelf, values of Ri_g are reduced when reaching the shelf break. The temperature data showed a vertical motion that appears to be related to the mechanism described by Wang (1984). In a rotating fluid over a sloping bottom, when two different water masses form a sharp density front, it stretches out from its initial position due to a reduction in the bottom layer velocity due to friction, increasing the relative velocity in the top layer. Assuming that no mixing occurs, the density structure is a layer of lighter water overlaying a layer of heavier water. The resulting velocity distribution is a relatively strong recirculation, with sinking at the head of the surface front and rising at the head of the bottom front. In the observations, however, there is no indication of vertical intrusion, since the density contours remain partially stable, but vertical stretching is observed (c.f., Fig. 3.1). A

baroclinic alongshore jet can be generated due to the geostrophic adjustment at the front. This is consistent with the increased $\partial v/\partial z$ at the offshore limit of the plume and the fact that the La Plata River plume advection is nearly geostrophic (Pimenta et al., 2005). The occurrence of this mechanism at the bulge of the plume, the region where the river water outflow transitions into a geostrophic or wind-dominated far-field, suggests that the La Plata River plume owns a mid-field region, which is not usually expected for large-scale plumes.

Therefore, results show that plume stratification inhibits larger mixing at the Albardão region. Further north in the Sta. Marta region reduced stratification facilitates the generation of shear-stratified turbulence, increasing levels of diffusivity at the plume boundary. Moreover, our observations suggest the presence of a unstable mid-field region.

3.1.3 Heat eddy diffusivity as a tracer for turbulent mixing in a estuarine plume

As explained in section 1.2.2.2, DDC may be an important factor for mixing at subsurface levels in the ocean. In some of the SBS profiles, the vertical distributions of TS suggest favorable conditions for double-diffusive processes. Areas affected by PPW are DR favorable, while at the shelf break SFR may occur. The TS distributions at the shelf break, such as in AL08 and SM01, together with the reduction in density overturns at the thermocline plus R_ρ above unity, suggest favorable condition for generation of salt-finger mixing. Moreover, at the thermocline, small-scale layers that resemble TS staircases (c.f., Fig. 1.5) can be seen, which is a possible indicative of active SFR. Within the plume interface, however, salt transport in the form of SFR is very unlikely to occur, since it only develops when salt is the destabilizing component, i.e., warmer saltier water above cooler fresher water (Kunze, 2003), such as in the Mediterranean outflow (Schmitt, 1994). In the present case, salt is a strong and effective stabilizing component of buoyancy, upholding colder waters at surface layers. Alternatively, DR may arise in the plume interface, as cold, fresher waters are in the surface layer. However, the strong buoyant and advection will unlikely allow a efficient heat loss by molecular diffusion. Moreover, there is no clear evidence of staircases layers at profiles made within the PPW. The heat diffusion by DDC is more frequently found in high latitude precipitation zones, such as the Arctic Ocean and sites around Antarctica, and salt stratified lakes with geothermal or solar heating (Schmitt, 1994; Kelley et al., 2003). But those regions differ greatly to a highly dynamic region such as the La Plata River plume. Hence, DDC is unlikely to be a relevant process in diapycnal mixing in the La Plata River plume.

A estuarine/river plume will become increasingly diluted as it propagates away

from its source region, characterized by decreasing density gradients between the plume and oceanic waters, owing to the increase diapycnal transports of salt and heat (Horner-Devine et al., 2015). However, freshwater dilution accounts for turbulent processes, such as the stirring due to tides, winds and bottom friction. Therefore, the transports of heat and salt are mainly driven by turbulence at the interface. It is assumed here that diapycnal diffusivity in the La Plata River plume interface can be estimated by temperature alone, as it is passively transported across isopycnals due to shear-stratified instabilities. In turbulent field with low Ri_g , the eddy diffusivities of salt and heat are very similar (Schmitt, 2003). The increase in K_T found in the SM profiles was a possibly a consequence of increased shear-stratified turbulence in the form of KH billows, as increased density overturns are observed. The increased instabilities resulted from the reduced stratification at the far-field region of the La Plata plume, where it is more susceptible to ambient stirring. Increased levels of K_T were also found at fully vertical mixed profiles close to the coast and at surface levels in the shelf break profiles. i.e., away from PPW influence. The disruption of temperature gradients in a turbulent profile can be expressed by K_T and B_f (and both are estimated from χ_T), and can be a quantitative measure of mixing in the absence of shear variance. Reliable estimates of temperature variance can indeed produce estimates of diapycnal turbulence from heat (e.g., Luketina and Imberger, 1989; Steinbuck et al., 2009; Fernández-Castro et al., 2014).

3.1.4 Part I conclusions

Our results show how the large-scale La Plata River plume affects vertical mixing in the shallow and dynamic SBS. Our observations are limited to two cruises of opportunity during Autumn conditions. However, two important conclusions may be drawn: (1) the transects in the SBS represent two distinct scenarios, as one was made close to the source region of the plume, where stratification due to freshwaters is very strong, and the other made a hundred of kilometers away from it, where the freshwater outflow is more diluted with oceanic waters. In this sense, both show differences regarding shear-induced variability in the interface with oceanic waters, expressed by the density displacements and magnitudes of heat diffusivity. Near the source region, the plume is highly stable, while away from the plume, going northward, shear instabilities are significantly increased; (2) the instability observed in the hydrographic data close to the shelf break, associated with low values of gradient Richardson number, suggests that the large-scale La Plata plume has a mid-field region of turbulence mixing, besides the far-field region located in the vicinity of Sta. Marta Cape. At the mid-field, data suggests that instabilities due to overturns in a sloping bottom is a source of turbulence, while in the far-field, KH instabilities are the causes of larger K_T .

Given the limitations imposed by the logistic of opportunity cruises and the limitations of our observations, this study is an initial contribution to the knowledge of the La Plata River plume dynamics and provide a good base for future turbulence studies in this important region in the southwestern Atlantic Ocean. More detailed surveys in the area are necessary in order to fully characterize the turbulent mixing of the La Plata River plume. Future investigations may include:

- In order to verify closely the possible implications of the BCC on the turbulent pattern in the coastal areas of the SBS, data must be obtained in areas between the AL and SM transects during SW winds regime. This would allow us to determine how this current can alter the shape of the turbulence within the plume;
- Obtain profiles of microstructure data near the entrance of the La Plata estuary, which could provide important information regarding the dynamics of the estuarine outflow at the source region;
- Verify the implications of seasonal changes in the wind field and discharge rate of the La Plata estuary on the plume turbulence pattern;
- Although to assume K_ρ similar to K_T is a valid approximation in a turbulent scenario, it would be interesting to obtain estimates of the salt eddy diffusivity in the plume interface to complement the results obtained here;
- Obtain measurements of ϵ from velocity shear variance, measured with shear probes (as those were not available during the survey herein) to estimate flux coefficient and mixing efficiency in the plume interface.

3.2 Part II: turbulent mixing induced by topographic features in the Vitória-Trindade ridge during Austral summer

3.2.1 Field observations

In Fig. 3.18 is show a perspective view of the VTR bathymetry from ETOPO2 (panel (a)), with the location of the main topographic features. The map highlights the large local bathymetric variability, with abrupt changes within a relatively short spatial scale. The quantitative measure of this the variability is given by the topographic roughness (panel (b)). Sharp topography is seen at the flanks of seamounts and banks of the ridge, as well as the area of the continental slope/ shelf break north of Abrolhos Bank. At these sites, increased interaction with the circulation is expected.

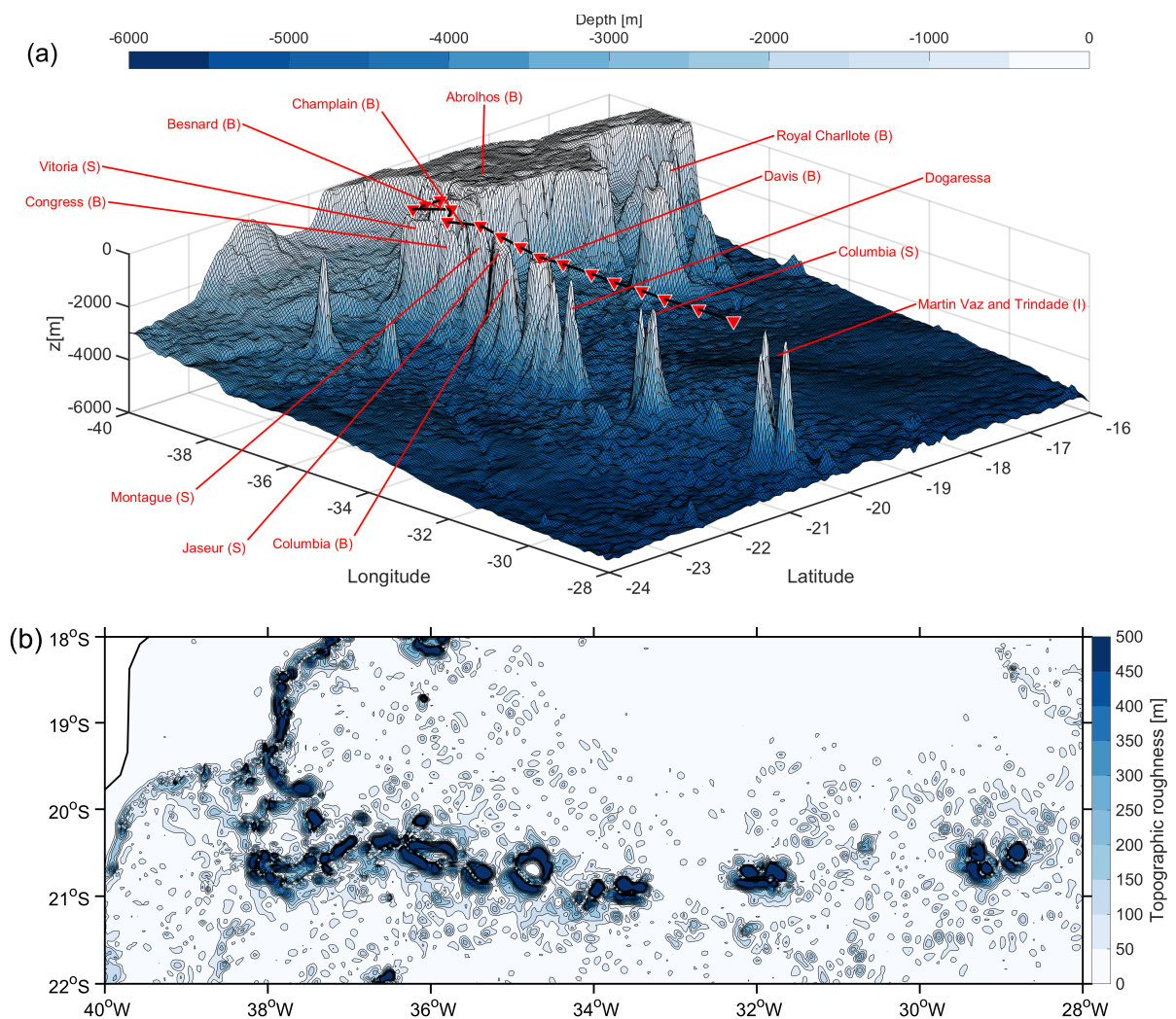


Fig. 3.18: Panel (a): perspective view of VTR bathymetry from ETOPO2 with location of the main seamounts (S) and banks (B). The black line is the transect's path and the red triangles are the oceanographic stations. Panel (b): map of estimated topographic roughness (r) for the VTR.

As expected for a subtropical, quiescent region, specially during summer, both heat and wind dynamics were very weak and nearly constant, with no great changes during the survey (Fig. 3.19). The net heat flux time series (panel (a)) shows the diurnal cycle of cooling and heating, with convective mixing at night and thermal stability during the day. The wind shear (panel b) was weak during the survey and thus did not affected significantly the surface mixing. In such conditions, convection may be an important contributor to vertical mixing in the SML [e.g., Shay and Gregg (1986)].

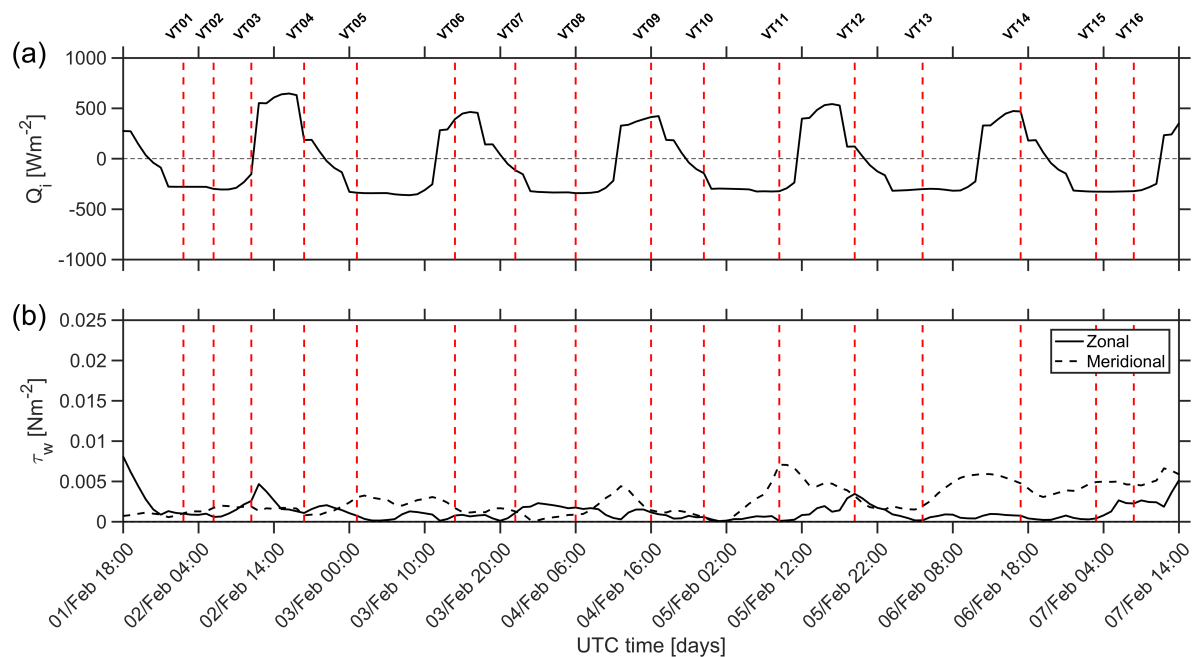


Fig. 3.19: Spatially averaged hourly time series of (a) net heat flux and (b) wind shear for the VTR region. The red dashed lines are the time of each station.

A high resolution transect of potential density obtained from the UCTD is shown in Fig. 3.20. The underway hydrography sampling was interrupted due to the lost of the SeaBird probe after station VT14. The data shows frequent oscillations along the isopycnals, particularly at the base of the SML, which varies significantly along the transect. Such variation is related to increased instabilities when approaching the seamounts, mostly between VT01 and VT06, where large vertical displacements of isopycnals are observed. Between Congress Bank (CON) and Montague Seamount (MON) isopycnals appear to be sinking from the base of the SML down to $\sim 200\text{m}$, increasing the SML depth. An increase in subsurface oscillations is seen within the depths of $\sim 150\text{-}300\text{ m}$, between VT13 and VT14, north of the summit of the Columbia Seamount (COL). A doming of isopycnals is observed at, approximately, 125 m, while a sinking of isopycnals is observed at around 250 m.

Away from the seamounts, there is no significant variation of the SML. As mentioned previously, the VTR region has significant mesoscale activity, but the most coherent mesoscale features are seen near the continental shelf off Abrolhos and Royal-

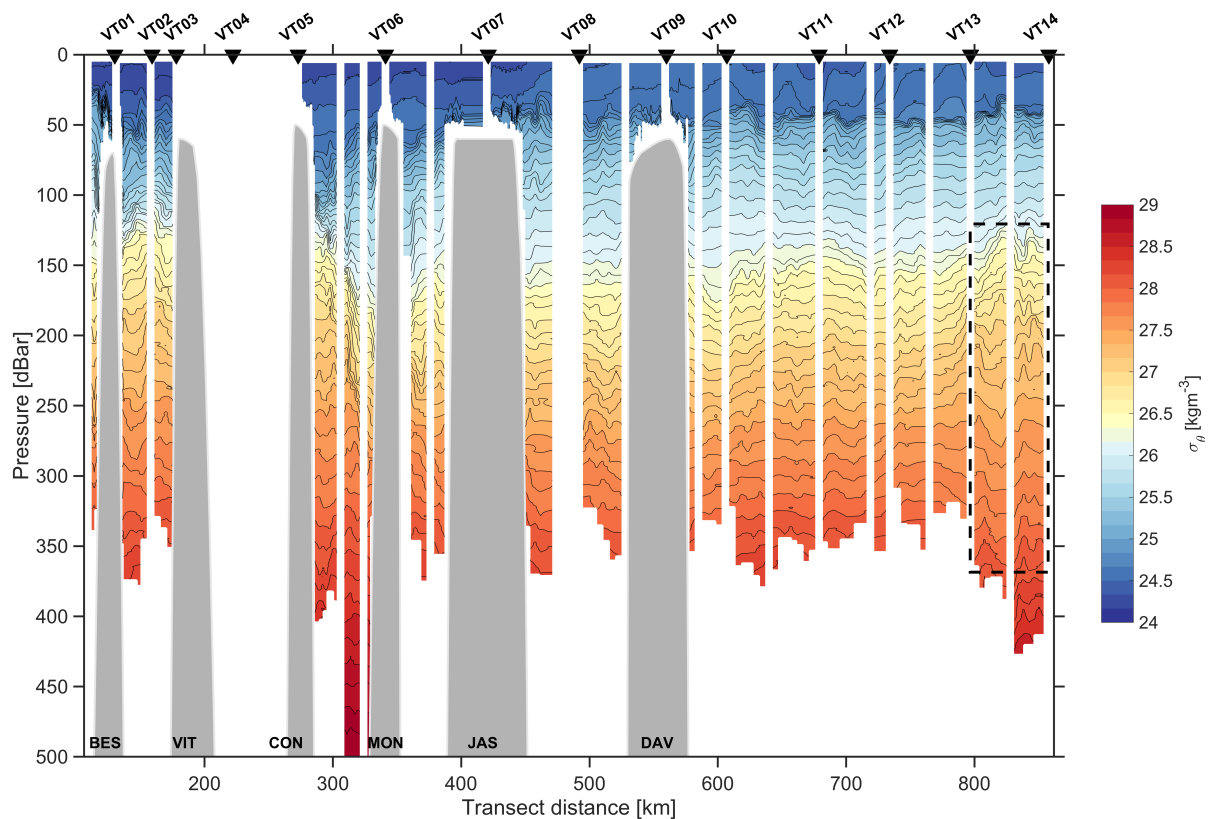


Fig. 3.20: High resolution potential density (σ_θ) obtained with the UCTD. The black rectangle highlights the doming of isopycnals observed at subsurface levels. The acronyms stand for: (BES) Besnard Bank, (VIT) Vitória Seamount, (CON) Congress Bank, (MON) Montague Seamount, (JAS) Jaseur Seamount and (DAV) Davis Bank. There is no data available after station VT14 because the UCTD probe was lost.

Charlotte Banks. This is corroborated by Fig. 3.21, which shows SSH anomalies and associated geostrophic velocities for Feb 6 2017. This date was selected because corresponds to the date when was detected the subsurface doming of isopycnals between VT13 and VT14. Moreover, no significant changes in the surface circulation occurred during the cruise, thus one image can be representative of the period. From VT07 to VT16, no discernible mesoscale activity is observed in the SSH image, which suggests that the doming of isopycnals is a intra-thermocline feature.

Mesoscale activity is evident from the spatial variability of the horizontal velocities (Fig 3.22), particularly in the western part of the transect, between VT01 and VT06, where velocities, isopycnal displacements and SSH anomalies are increased (c.f. Fig. 3.20 and 3.21). Zonal currents reach $\sim 0.5 \text{ ms}^{-1}$ near the summit of the Vitória Seamount (VIT) and at $\sim 400 \text{ m}$ between this seamount and the Besnard Bank (BES). A strong northward component is also observed at Jaseur Seamount (JAS). Both horizontal velocities and isopycnal variability are significantly reduced away from the seamounts ($\sim 0.1 \text{ ms}^{-1}$). However, between stations VT13 and VT14, increased horizontal velocities are observed within the $\sim 150\text{-}300 \text{ m}$ depth interval.

The frequency of occurrence of ϵ , K_ρ , R_ρ and Γ (Fig. 3.23) were clustered into data

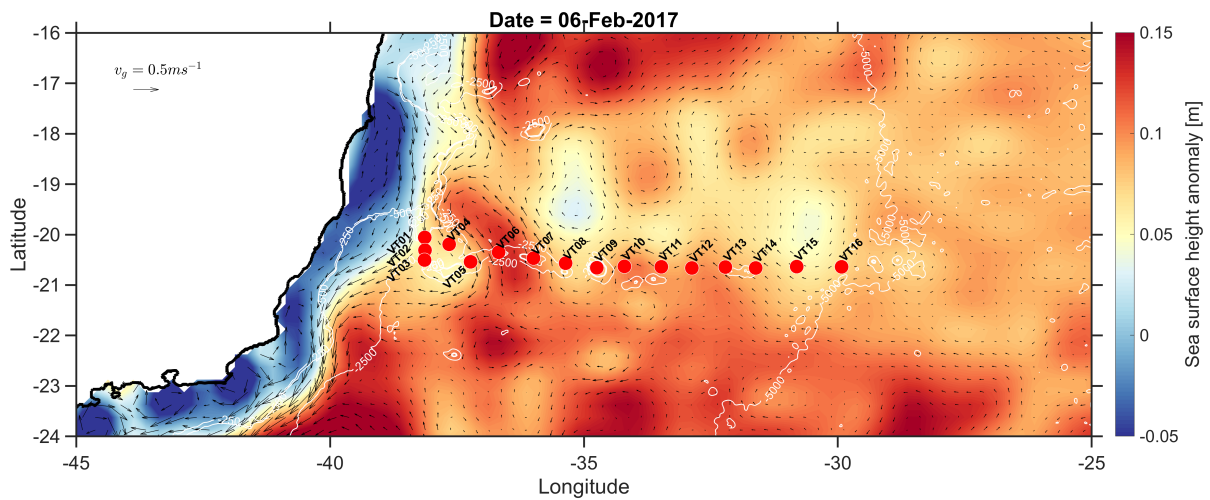


Fig. 3.21: Sea-level satellite altimetry anomalies plus geostrophic velocities from the AVISO database for Feb 6 in the VTR region.

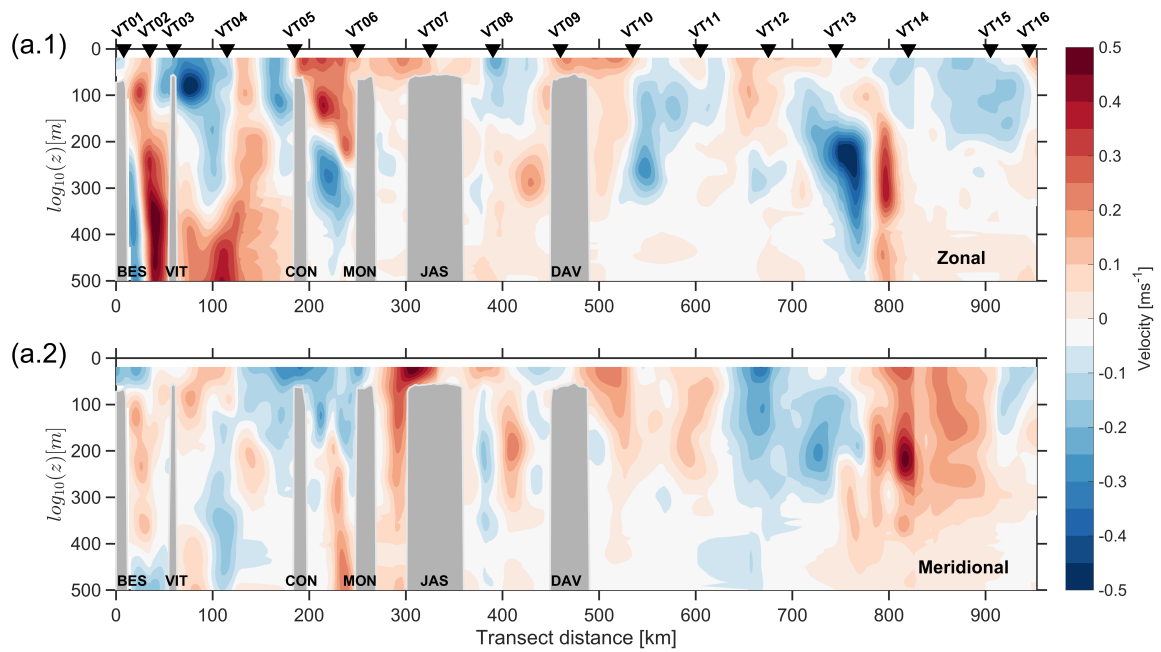


Fig. 3.22: Zonal (a.1) and meridional (a.2) current velocities along the VTR obtained with the onboard ADCP. Positive (red) zonal and meridional velocities are east and northward, respectively.

collected in the SML (assumed to be less than 70 m) and the ocean interior (OI). In the SML, distributions are nearly bi-modal for dissipation (panel (a)) and diffusivity (panel (b)), while their shape is close to Gaussian in the OI. The bi-modal shape is result of increased values of ϵ and K_ρ closer to the surface. On average, turbulence was almost one order of magnitude higher in the SML than in the OI. The modes and averages of each distributions are displayed in Fig. 3.23. The R_ρ distributions (panel (c)) for SML and OI were similar, with the modes at ~ 1.6 for both. The high surface temperatures, ubiquitous in latitudes of the VTR, mainly during summer, leads to increase evaporation and, hence, high surface salinity. Thus, as both background temperature and salinity

decrease with depth, favorable conditions for SFR arise. This corroborates with much of the salt finger favorable upper ocean waters at tropical, subtropical and mid-latitudes [Kunze (2003)].

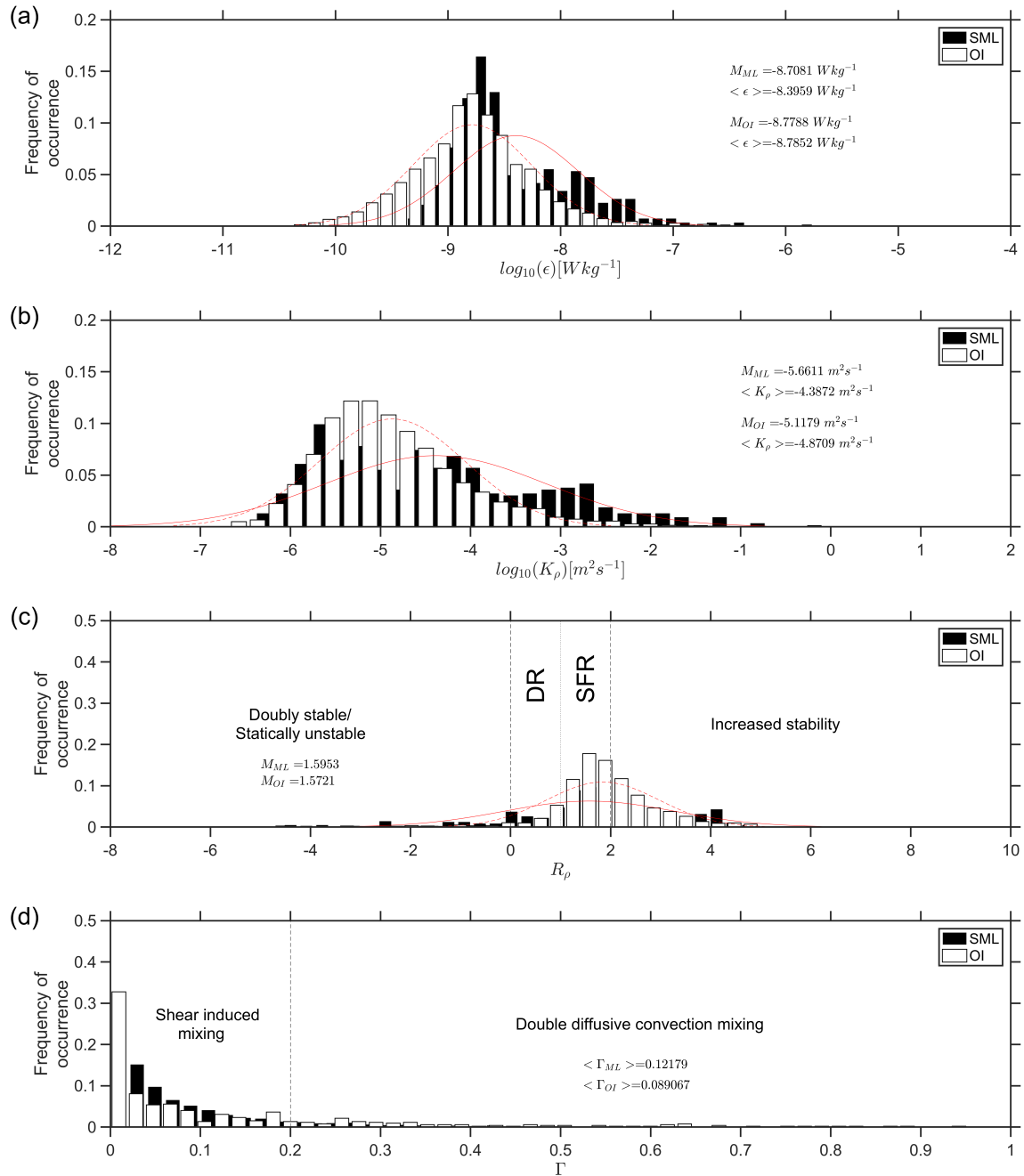


Fig. 3.23: Frequency of occurrence of (a) ϵ , (b) K_{ρ} , (c) R_{ρ} and (d) Γ computed within the surface mixed layer (SML, < 70 m) and ocean interior (OI). In panel (c), DR stands for diffusive regime and SFR for salt-finger regime and the vertical dashed line refer to the thresholds within each type of DDC regime is prone to occur. The vertical dashed line in (d) is the threshold between shear-generated and diffusive convection mixing, i.e., $\Gamma = 0.2$. The red lines are the log-normal probability functions fitted to the data (full for SML, dashed for OI).

The distribution of the flux coefficient, Γ , shows that shear is the main source of mixing in the VTR. Mixing by DDC (mainly salt-fingers) represents a small fraction of

the total amount of mixing. In the OI, about 11% of Γ values were above 0.2, which increases to about 17% when Γ is computed for data in the SML. This means that mixing by DDC is slightly larger close to the surface. This small increase is due to (1) the values in the thermocline, where the probability of DDC generation increases because of larger stability/slower dynamics and (2) the lower magnitude of shear variance. As within the SML the potential energy gain due to vertical mixing is significantly larger than in the OI, the average Γ is ~ 0.12 , while in the OI the average is ~ 0.09 .

The contribution of convection to ϵ in the VTR was verified through linear regression between B_f and ϵ (Fig. 3.24). When computed over all data (panel (a.1)), the regression shows that about 31% of the magnitude of dissipation is related to buoyancy flux, which increases to around 63% when the regression is computed with data from the first 70 m (panel (a.2)). This demonstrates the importance of convection on uphold surface mixing, specially in regions where temperature is the main mechanism controlling buoyancy. The linear regression between K_ρ and K_T computed over all data points (panel (b.1)) yielded about 58% of correspondence, increasing to almost 88% within the first 70 m (panel (b.2)). As turbulence is the main mechanism driving mixing, heat eddy diffusivity is very similar to density diffusivity [Schmitt (2003)].

The estimates of the efficiency of turbulent mixing in the VTR are shown in Fig 3.25, expressed by Richardson flux number as a function of the turbulent Froude number. The most effective turbulence, where R_f falls between 0.15 – 0.25, usually occurs at $Fr_t \approx 1$ [e.g., Ivey and Imberger (1991)]. Most points were located between 0 and 0.25 for Ri_f and 0.2 and 2 for Fr_t . High values of both R_f and Fr_t were associated with low N , i.e., SML, where usually turbulence is highly inefficient because any shear input within a vertically mixed water column will only result in dissipation into heat. Lower values with high N can be related to the thermocline, where stratification is strong and ϵ is usually low. Fr_t is, in general, reduced where N is enhanced. At the thermocline, stratification overcomes shear significantly, reducing Fr_t , and when shear production is not capable of overcome buoyancy, it results in low efficiency. Most values found within the optimum range for efficiency were found at moderate stratification associated with subsurface levels. For data obtained at depths less than 70 m, efficiency appears to be patched at strong (thermocline) and weak (SML) stratification, with few points are located in the optimum range.

Fig. 3.26 shows profiles of ϵ and K_ρ obtained at each station. Larger values of dissipation and diffusivity are observed in the upper ~ 50 -70 m, as turbulence is increased near the air-sea interface due to convection and wind shear. The weak atmospheric forcing during the survey resulted in a nearly constant SML depth, as seen in the σ_θ transect (c.f. Fig. 3.20). Even so, the variation of the wind shear plus nighttime convection yielded peaks of dissipation (e.g., station VT16). At shallow stations on top of the seamounts and banks, vertical mixing is larger than surroundings due to increased

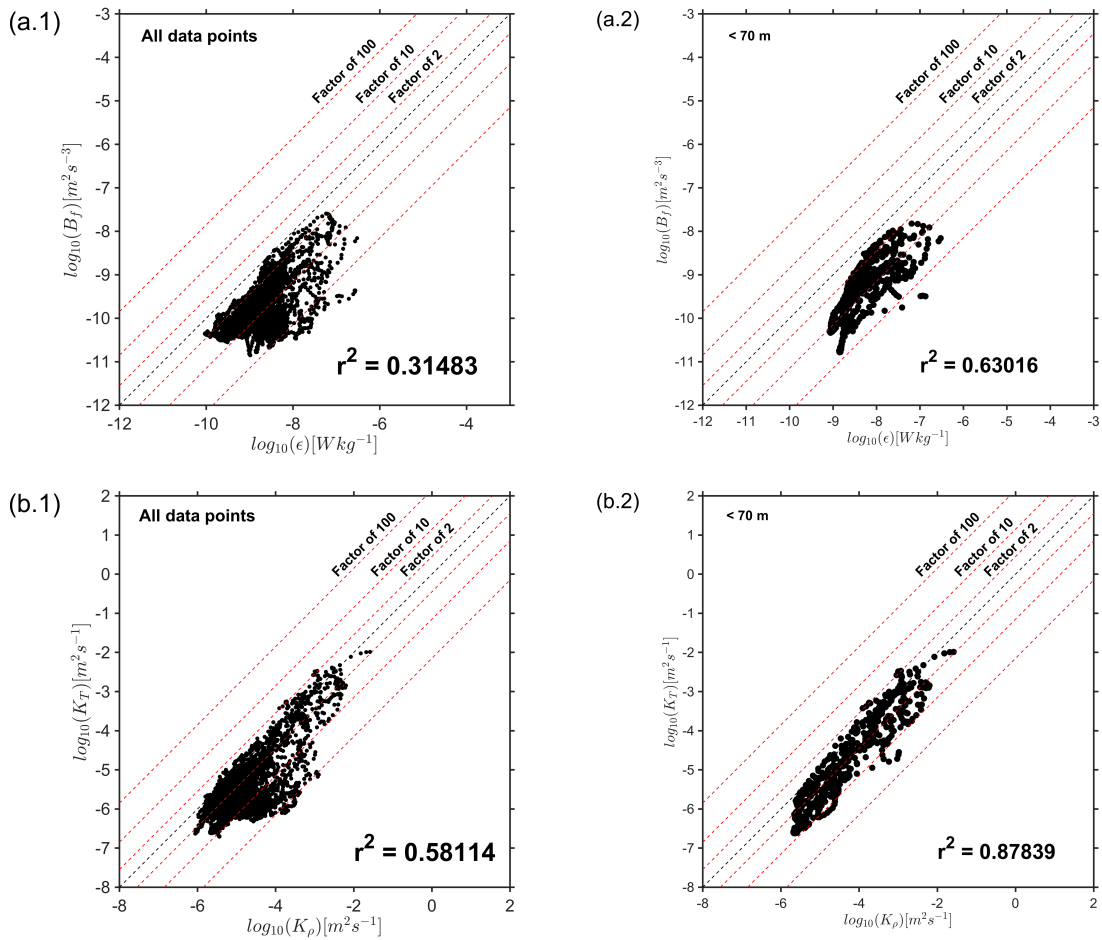


Fig. 3.24: Linear regressions between (a) $\log_{10}(B_f)$ and $\log_{10}(\epsilon)$ and (b) $\log_{10}(K_\rho)$ and $\log_{10}(K_T)$. In (a.1) and (b.1) are the regressions over all data points and (a.2) and (b.2) are for the first 70 m. The dashed black line is a perfect fit and the red dashed lines are deviations under and above the perfect fit by an order of 2, 10 and 100.

currents and their interaction with the topography. In addition, both ϵ and K_ρ profiles reveal enhanced turbulence at VT13, in the subsurface levels within ~ 250 - 300 m. The turbulent patch together with the spreading of isopycnals and the strong horizontal velocities, indicate an active mixing in the vicinity of COL. This highlights the importance of flow-topography interactions in generating high levels of subsurface turbulence. At station VT13 high levels of dissipation and diffusivity are observed, with magnitudes of $\mathcal{O}(10^{-7}) - \mathcal{O}(10^{-6}) \text{ Wkg}^{-1}$ and $\mathcal{O}(10^{-2}) - \mathcal{O}(10^{-1}) \text{ m}^2\text{s}^{-1}$, respectively, mostly within pycnoclinic levels between 26.75 and 27.5 kgm^{-3} .

Since the patch of subsurface mixing was only observed in VT13, a detailed view is shown in Fig. 3.27. The profile may be separated into four segments with different turbulent characteristics: a fully mixed surface layer, a quiescent layer between ~ 50 - 150 m, a subsurface stratified layer between ~ 150 - 225 and a homogeneous turbulent layer between ~ 225 - 275 m. No relevant discernible features are seen deeper. Within the SML, shear variance is large, but both χ_T and L_T (panels (b) and (c), respectively)

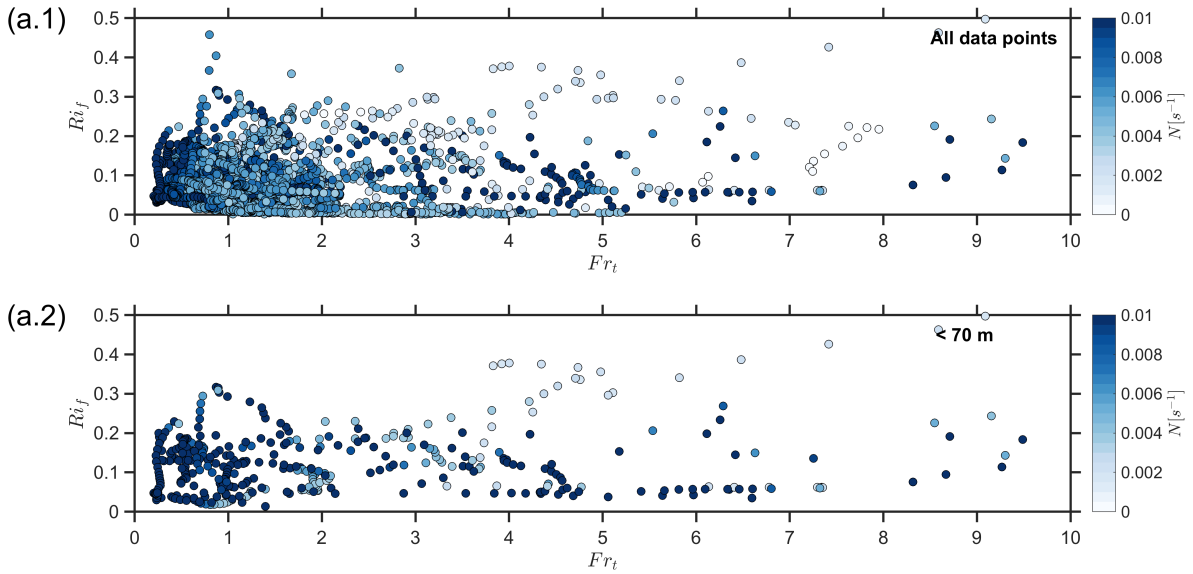


Fig. 3.25: Distributions of Ri_f as a function of Fr_t for (a.1) all data points and (a.2) the first 70 m. The colorbar refers to N associated with each point.

are very low. This is an indication of the absence of stratified layers and, therefore, any shear input is only being dissipated as heat and no active mixing is occurring, i.e., low efficiency (c.f., Fig. 3.25). The B_f/ϵ profile (panel (a)) shows that B_f is occurring due to convection, but overall dissipation overcomes the buoyancy flux, i.e., high shear production. σ_θ is practically homogeneous, hence N^2 is nearly zero (panel (d)). The top of the quiescent layer (i.e., the thermocline) is highly stratified due to temperature gradients. χ_T is increased, but both L_T and shear variance are reduced, which shows that the layer is stable. Below the thermocline, velocities are slightly increased (panel (e)), but are still low and no significant shear variance arises. χ_T and L_T are very low, as no significant gradients are observed. B_f/ϵ is practically zero, as no buoyancy production is occurring. This is an opposite situation of the one occurring in the SML, but now the shear is not capable of overcome stratification and, again, efficiency is low (c.f., Fig. 3.25). σ_θ increases monotonically with depth and N^2 varies accordingly, but remains close to zero as within the SML. At about 150 m deep, χ_T and L_T increase abruptly. Shear variance increases slightly, but it is greatly surpassed by B_f , suggesting that buoyancy is being generated within the layer, hence increasing N^2 . This is the approximate depth at which isopycnals start to spread vertically and horizontal velocities start to increase significantly. The layer between ~ 225 - 275 shows large shear variance, increased χ_T and L_T . This is indicative of active (and efficient) turbulence, as shear input is being used against density gradients to yield vertical mixing, as opposed to the SML. The large negative peak in B_f/ϵ suggests a strong downward heat flux, implying that vertical heat fluxes are strong and active within the layer. As a result, N^2 is nearly zero.

A close-up in the horizontal velocities and the σ_θ section (Fig. 3.27, (f) and (g))

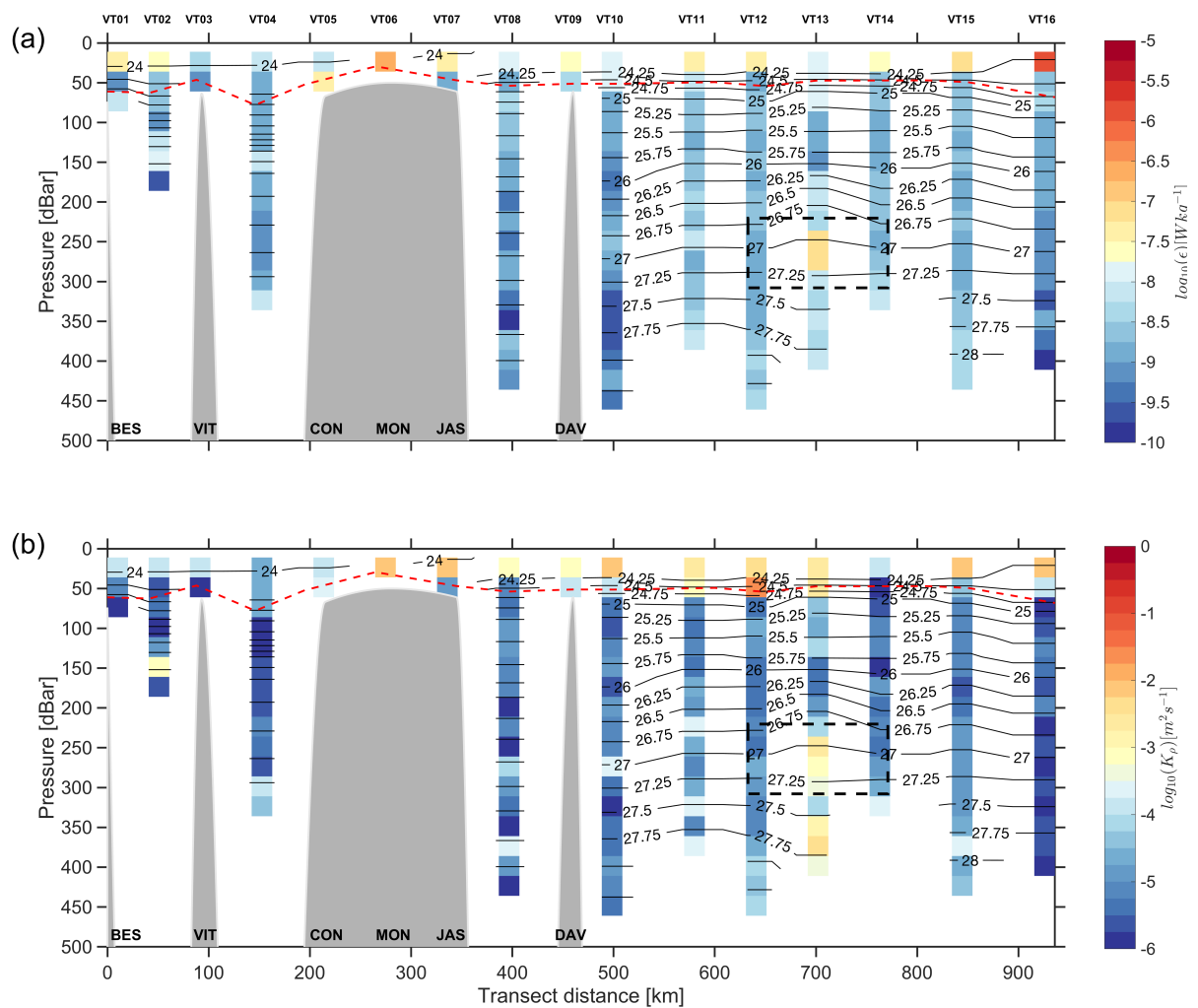


Fig. 3.26: Log_{10} profiles of (a) ϵ and (b) K_ρ obtained in the VTR survey. The black lines are the isopycnals in kg m^{-3} and the red dashed line is the SML depth. The black rectangle highlights the enhanced turbulence found at subsurface levels.

above to stations VT13 and VT14, adjusted to the time of the profiles, shows that oscillations increase significantly in amplitude, mainly within the 26.3 kg m^{-3} to 27.5 kg m^{-3} isopycnal interval. Those increased oscillations are coherent with an divergence of horizontal velocities. Close to the northern flank of COL, the vertical displacements of isopycnals becomes more vigorous and horizontal velocities become larger. Visually, the section shows what appears to be an internal wave of approximately 15 m of height, with a period of approximately 3 hours. If this is the case, the high subsurface TKE dissipation at VT13 may be indicative of internal wave breaking, as a consequence of interaction with the topography.

3.2.2 Turbulent mixing in the VTR region

The VTR is in a region where the high surface heat induces relatively strong stratification, specially during summer. Hence, it suggests an overall vertical stability.

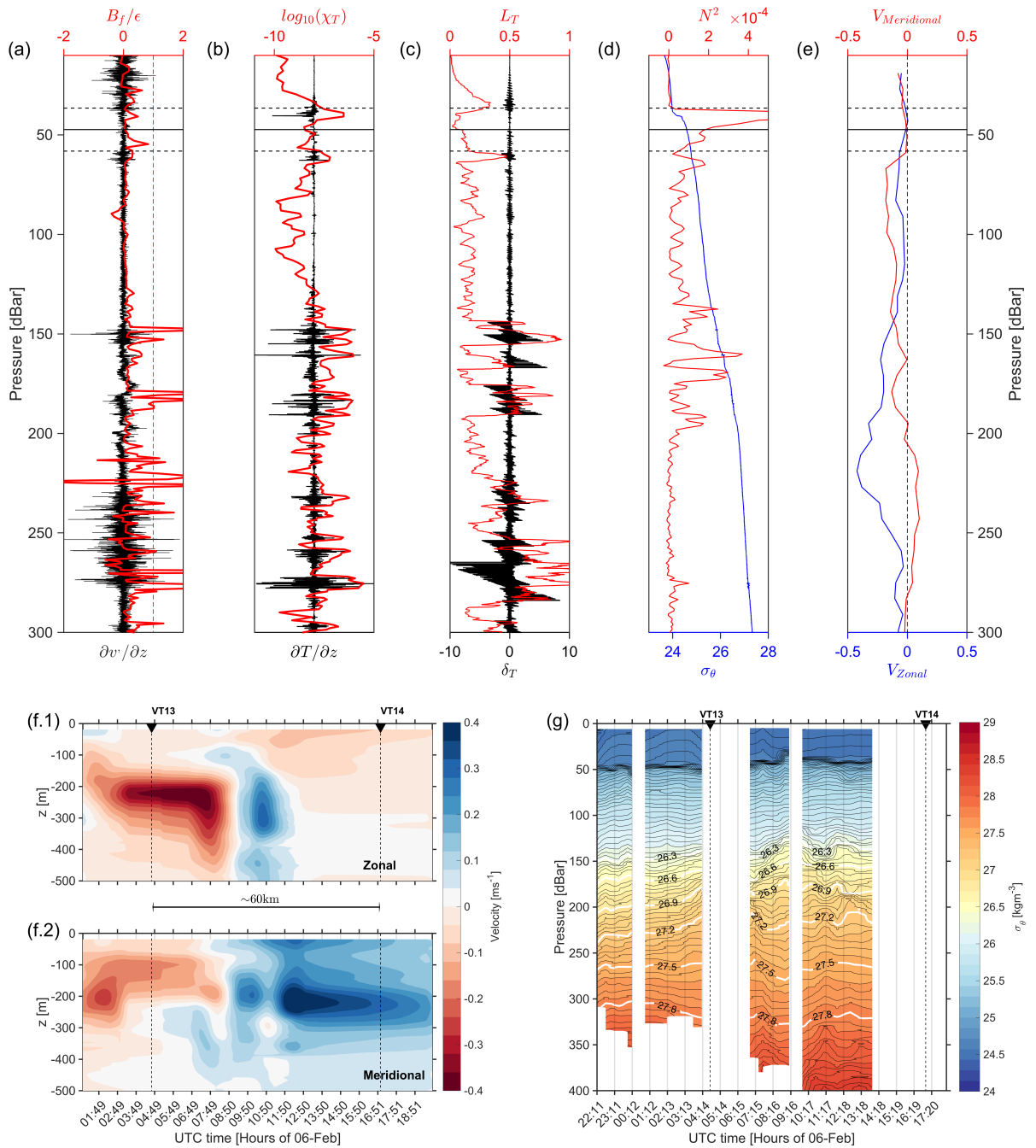


Fig. 3.27: Detailed view of profile VT13; In (a) is the microstructure velocity shear variance ($\partial v' / \partial z$, black), along with B_f / ϵ (red); in (b) is the microstructure temperature gradient (black), together with the temperature variance (χ_T , red); in (c) are the density overturns (δT , black) and respective Thorpe length scales (L_T , red); in (d) are the profiles of N^2 (red) and σ_θ (blue); in (e) the zonal (blue) and meridional (red) velocity profiles; in (f) and (g) is a close up of the horizontal velocities and the σ_θ section, respectively, at the location of the subsurface mixing patch, adjusted to the time of each profile. The dashed line in (a) is $B_f / \epsilon = 1$ and the horizontal black line is the SML depth calculated for this profile. The white lines in (g) are to highlight the oscillations of isopycnals.

However, when considering mesoscales to small-scales, mixing processes can be observed. Earlier studies demonstrated that the region is dominated by mesoscale activity, since the VTR is one of the first contact points of the BC to the Brazilian shelf [e.g.,

Da Silveira et al. (2004); Soutelino et al. (2011, 2013); Arruda et al. (2013)]. When such large and energetic western-boundary current reaches the continental shelf and encounters a region with a such a complex and variable bathymetry, it causes the re-distribution of energy in the form of mesoscale circulation features, e.g., cyclonic and anti-cyclonic eddies. The velocity transect for both zonal and meridional components and SSH data demonstrated this mesoscale variability. The UCTD data also show the presence of oscillations that resemble internal waves, specially at the location of the subsurface turbulent patch. Therefore, the VTR may subject to different patterns of turbulence from different sources, being sometimes endemic to the region, as well as transitory.

The correspondence of B_f and ϵ found in the linear regressions remarks the importance of heat fluxes on generating mixing at the surface, specially at mid to low latitudes regions where winds are generally weak and surface heat is high, such as the VTR.

To determine the efficiency of turbulence using microstructure data from the open ocean may be problematic. Most studies that evaluate efficiency use experimental data, and large variability is usually disregarded [e.g., Ivey and Imberger (1991); Moum (1996); Smyth et al. (2001)]. In spite of the large variability, the present observations provided a rough estimative of efficiency of the VTR turbulence. R_f relates the relation of buoyancy and shear production based on the flux coefficient, and Fr_t is a ratio between the scales of the turbulent eddies and the density overturns. Efficient turbulence is generated in stratified interfaces where shear magnitude is coherent with the strength of stratification, causing Ozmidov and Thorpe scales to have approximately the same order [Dillon (1982)]. In the SML, L_O is significantly higher than L_T , reducing effectiveness of mixing. On the opposite case, the overturns are much larger than shear, which means that the density variations will unlikely evolve into KH billows [Smyth and Moum (2000)].

3.2.2.1 Subsurface turbulence patch

One of the most interesting features found in the VTR survey was the strong levels of ϵ and K_ρ in the subsurface layer on the northern flank of a Columbia. The average dissipation and diffusivity found within the patch were $3.4 \times 10^{-8} \text{ Wkg}^{-1}$ and $2.1 \times 10^{-3} \text{ m}^2\text{s}^{-1}$, respectively, computed within the $\sim 150\text{-}300$ m depth range at VT13. These values were one order of magnitude larger than the averages for the entire transect excluding the SML, which were $2.5 \times 10^{-9} \text{ Wkg}^{-1}$ for ϵ and $1.2 \times 10^{-4} \text{ m}^2\text{s}^{-1}$ for K_ρ . Within the subsurface patch, a strong shear-induced turbulent heat flux occurred, yielding vertical density overturns, hence the large negative B_f and large χ_T . In order to restore stability, buoyancy works against shear, yielding large variability in the B_f/ϵ ratio. The microstructure temperature variance, χ_T , can be related to the presence and action

of turbulent motion when shear variance is observed simultaneously [Steinbuck et al. (2009)].

The subsurface shear may have been caused by a variety of mechanisms. Surface winds may provide conditions for subsurface instabilities, but it depends on the local depth and on the wind magnitude [Price and Weller (1986)]. The data do not support this hypothesis, since the turbulent patch is restricted to a specific subsurface layer and wind shear was not strong enough to induce instabilities at subsurface levels.

Another plausible hypothesis would be an eddy-type circulation interacting with the seamount topography. Previous work showed that the sSEC bifurcation is eddy-dominated from 15°S to 19°S [e.g., Schmid et al. (1995); Arruda et al. (2013); Soutelino et al. (2013)] and anticyclones related to the meandering of the BC suggest a flow influenced by the topography [Soutelino et al. (2011)]. The SSH anomaly map, however, does not show any significant mesoscale feature between VT13 and VT14, which suggest that the observed feature is restricted to subsurface levels. The shape of the isopycnals can be reminiscent of an Intra-Thermocline Eddy (ITE) [Riser and Owens (1986)], as seen by the doming isopycnals observed in both UCTD and VMP-250 profiles, as well as the large horizontal velocities. However, the velocity pattern does not resemble a coherent eddy structure.

Regions with abrupt topographic variations are usually prone to internal tides [Garrett and Kunze (2007); Lamb (2014); Legg (2016)], and significant semidiurnal internal tide activity occurs in the VTR in the vicinities of Abrolhos and Royal-Charlotte banks Pereira et al. (2005). Previous studies have associated the importance of internal tides on generating high levels of turbulence in regions of complex bathymetry [e.g., Toole et al. (1997); Carter et al. (2006); Hall et al. (2013); Wain et al. (2015)]. At near critical slopes (i.e., $\alpha \approx 1$), internal waves become nonlinear, leading to wave breaking and turbulent mixing [Ivey and Nokes (1989)]. As seen in Fig. 3.18, the VTR is composed of very sharp topographic variations, where steepness increases rapidly within a short distance, and the spatial distribution of α (Fig. 3.28) shows that near-critical slopes are found at the base and flanks of the seamounts in the ridge. The areas where $\alpha \approx 1$ are restricted to narrow regions, changing to supercritical within a few kilometers. The horizontal velocity pattern (Fig. 3.27, (f)) and the increased oscillations in the isopycnals (Fig. 3.27, (g)), show consistent evidence to support the presence of internal waves near COL.

The oscillations observed within ~ 150 -300 m were likely caused by the passage of an internal tide at the location of profile VT13. Internal tides may have been generated by the interaction of the barotropic tide with the near-critical slopes at the flanks of COL. The present observations are consistent with other studies that reported strong turbulence along the semidiurnal wave beam [e.g., Lueck and Mudge (1997); Lien and Gregg (2001); Carter et al. (2006)]. An example of a M_2 internal tide beam reflecting

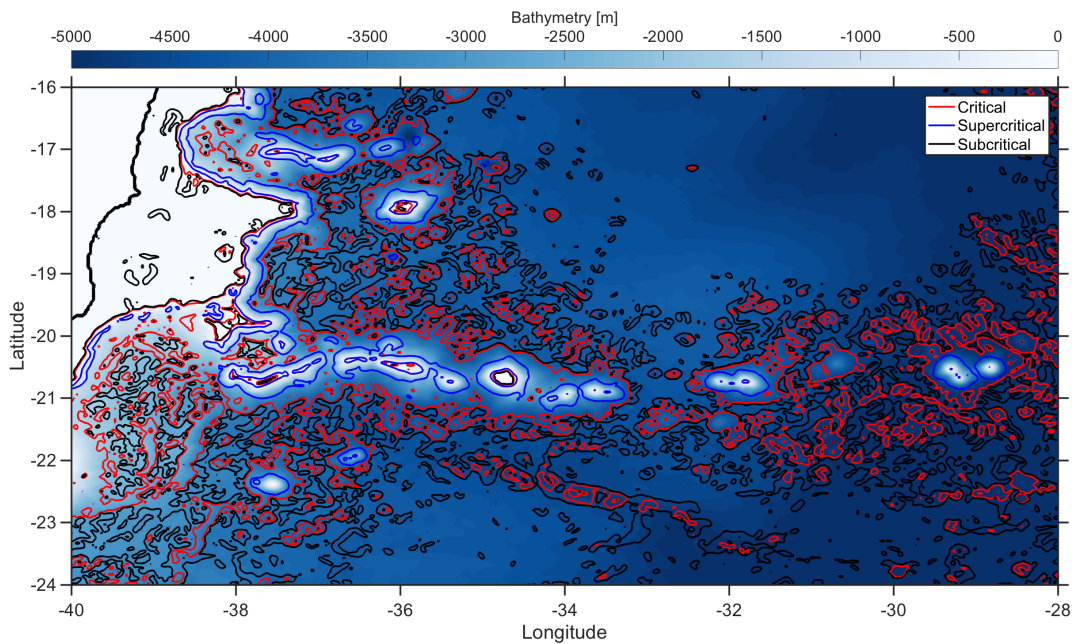


Fig. 3.28: Estimated topographic slope and wave characteristic slope ratio (α) plotted over the ETOPO2 bathymetry. The red contours are critical slopes ($\alpha \approx 1$), blue are supercritical ($\alpha > 1$) and black subcritical ($\alpha < 1$). The location of the Columbia Seamount is highlighted.

from critical slopes in the VTR is shown in Fig. 3.29. γ_{M_2} was calculated assuming $\omega = 1.4 \times 10^{-4} \text{ s}^{-1}$ (the angular frequency of the M_2 tidal component), $f = -5.56 \times 10^{-5} \text{ s}^{-1}$ and a climatological N^2 profile for the region. The resulting wave beam crosses the VT13 profile just above the observed turbulent patch. Therefore, internal tides as cause of the observed shear is the most reasonable hypothesis. The wave beam may have been generated at another location, since critical or near-critical topography is found all over the ridge. However, the shape of the Columbia Seamount and its relative isolation from the other topographic features of the ridge appears to yield ideal conditions for internal tide generation.

Simulations of reflected tidal beams generated near critical bathymetric slopes show that they tend to surpass the topography and induce instabilities [e.g., Johnston (2003); Sarkar and Scotti (2017)]. In the deep ocean, tidal velocities are generally very small, and flat topography tends to dissipate only a small amount of TKE. But when weak deep-ocean barotropic flow encounters steep topography, it induces a non-linear response, increased baroclinic velocities and the generation of small scales processes that cause turbulence [Legg (2016); Sarkar and Scotti (2017)].

3.2.3 Part II conclusions

The VTR is a potential site for mixing in the southwestern Atlantic Ocean due to the intricate circulation yield by the southern branch of the SEC and the complex bathymetry. The main source of turbulence in the ridge is the flow-topography inter-

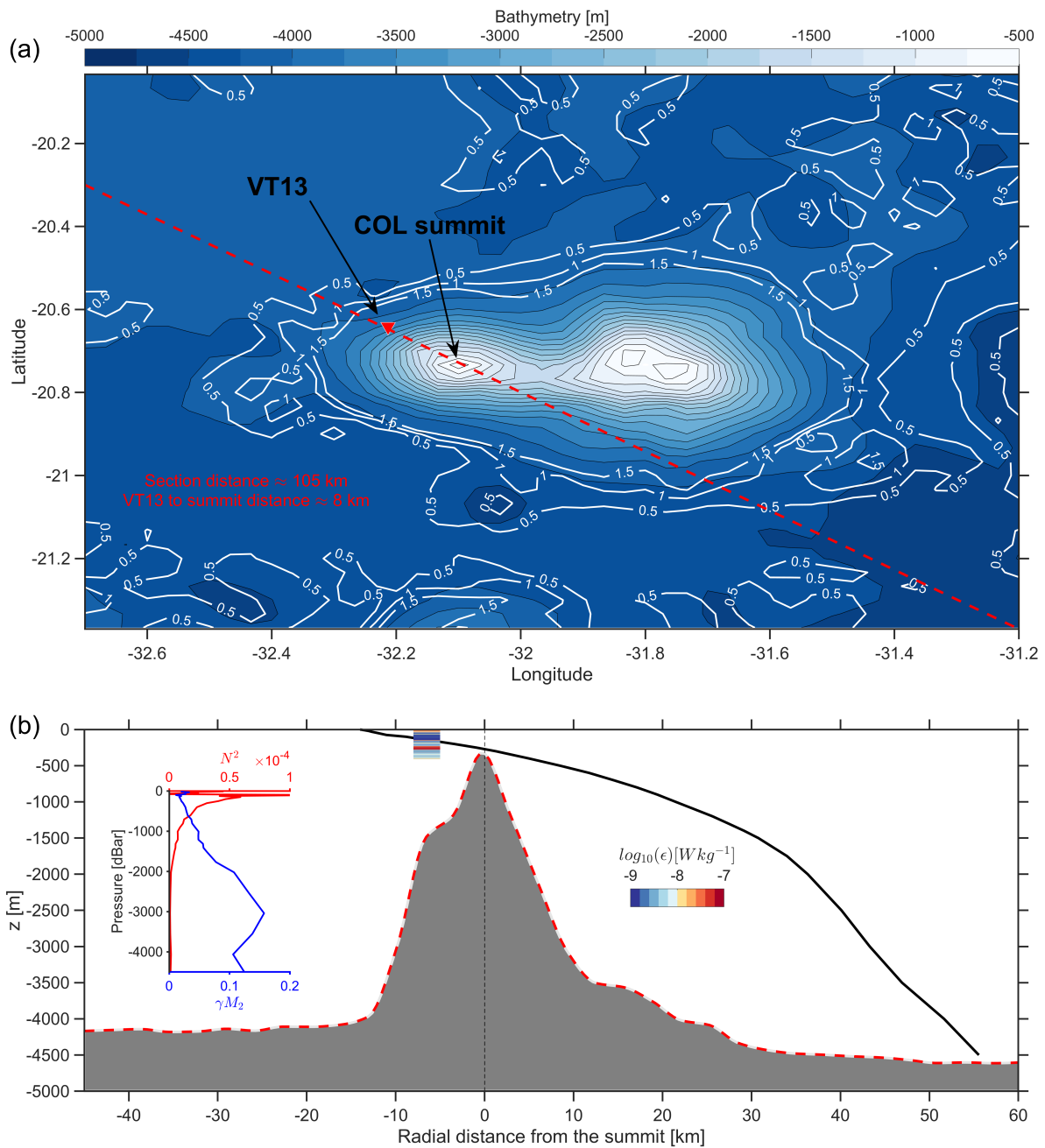


Fig. 3.29: In (a) bathymetry of COL and vicinities. The dashed red line is the topographic section across VT13 (upside down red triangle) and the seamount summit. The white contours are the areas of near-critical to critical slopes; in (b) side-view of the section showing the estimated beam path for the M_2 wave crossing the VT13 profile. The smaller panels show the vertical profiles of N^2 (red line) and γM_2 (blue line). The colorbar refers to the $\log_{10}(\epsilon)$ measured at the station.

actions. DDC may be developed, but accounted for a very small portion for overall mixing. Wind shear plays a role in surface mixing, but as the survey was made in summer in a normally quiescent region, most of surface mixing is associated with heat fluxes. Enhanced subsurface mixing was also observed within the ~ 150 - 275 m depth range, northwest of the Columbia Seamount. Although the VTR is a site of substantial mesoscale activity, the SSH anomaly maps and the ADCP data do not support the

presence of a coherent mesoscale eddy interacting with the topography. The most reasonable hypothesis is that the subsurface turbulent activity was generated by internal tides that emanated from the critical topographic slopes in the vicinity of the seamount.

More detailed observational and modeling studies should be performed in the region in order to determine the turbulence pattern associated with internal tide generation. The results suggest that the VTR is a potential hotspot for mixing in the Southwestern Atlantic Ocean. The fact mixing is induced at pycnoclinic levels may be relevant for nutrient supply in this oligotrophic region and help explain the high biodiversity associated with the seamount chain, with possible consequences for biogeochemistry in the region.

Chapter 4

Contribuição para a indústria do petróleo¹

O presente trabalho teve como objetivo caracterizar os processos turbulentos nas duas regiões de estudo. A Plataforma Continental Sul-Brasileira é uma região altamente dinâmica de alta importância econômica, não apenas pelos recursos disponíveis para a pesca comercial, mas também pelo intenso movimento de navios de grande porte. A Cadeia Vitória-Trindade por sua vez, pode parecer a princípio uma região oligotrófica, porém fora observado a importância da circulação gerada pela interação do escoamento com feições topográficas em gerar diversidade biológica ao redor dos montes submarinos e ilhas da cadeia. Para a indústria do petróleo, tanto na questão logística como na extração no oceano, o conhecimento dos processos de mistura, tanto em relação à sua intensidade como a identificação dos chamados 'hot spots' de turbulência, é de suma relevância. Os padrões de turbulência superficial podem influenciar a dispersão de óleo em caso de derramamentos e a localização dos 'hot spots' de mistura pode ajudar a reduzir os danos causados pela presença de petróleo no oceano, uma vez que essas áreas podem potencializar a dispersão devido a turbulência local. Na Plataforma Continental Sul-Brasileira a dinâmica devido a presença da pluma do Rio da Prata e ventos sazonais seguramente determinam como substâncias despejadas no oceano são advectadas e misturadas. Esta tese forneceu um panorama inicial de como a dinâmica da pluma pode afetar a mistura vertical e contribuir para o planejamento de operações de contenção. Já a descrição dos processos de mistura devido as interações com a topografia não apenas contribui para o entendimento dos processos de mistura superficial, mas também podem auxiliar as operações de extração de petróleo no fundo oceânico. Os padrões de turbulência junto ao fundo estão diretamente ligados a dinâmica do escoamento e a complexidade da topografia. Nesse âmbito, os resultados aqui presentes fornecem uma caracterização

¹Parte do Programa de Recursos Humanos (PRH-27) - Petrobrás e Agência Nacional do Petróleo

inicial dos processos de mistura ligados à topografia da Cadeia Vitória-Trindade que podem contribuir para a logística de extração de petróleo no oceano.

Chapter 5

Conclusions

This thesis presented the first observations of *in situ* turbulence performed at two very dynamic and complex regions in the southwestern Atlantic Ocean. The results demonstrated that both regions are subject to different forcings that lead to different forms of turbulence generation.

Several researchers along the years have proved the relevance of the SBS in the circulation in the south Atlantic basin by exploring its dynamics and respective implications to different fields. This continental shelf has a high socio-economical importance, mostly due to fisheries and commercial navigation. The overall circulation, both in the continental shelf and shelf break, is well elucidated due to substantial contributions of researchers from Brazil and Argentina. In a region of such importance and complexity, the quantification of turbulence, and most importantly, how does the La Plata River plume affects the vertical mixing, is of great value and contributes significantly to the characterization of the SBS. Two very important conclusions were obtained in the SBS survey: (1) the plume strong stratification reduces shear-induced turbulence at southern areas of the shelf and (2) the La Plata plume owns a dynamic mid-field region. Therefore, In spite of the limitations, a base for turbulence studies in the SBS is now available.

The VTR is one of the first locations encountered by the southern limb of the BC when reaching the Brazilian continental shelf, and the energy transferred from the larger scales towards mesoscales and submesoscales have direct implications on circulation and hence, turbulent mixing patterns in the ridge. As the survey was made during austral summer, mostly of the surface mixing accounts for heat fluxes. However, increased dissipation was found when reaching areas close to the continental shelf, where topography is even more complex. The subsurface mixing patch near Columbia Seamount is a good example on how isolated topographic features may lead to enhanced turbulence activity in the ocean when compared to surrounding areas. Moreover, the results corroborated with previous studies that demonstrated that the VTR is (1) an important site of internal tide activity and is (2) a hotspot for mixing in the south-

western Atlantic, with possible implications to the local biological productivity. Given the potential importance of the VTR for turbulence generation and, consequently, the overall circulation of the South Atlantic Ocean, more detailed observational surveys should be performed in the region. This would allow to determine the role of the topographic features in generating turbulence in the area, as well as the potential consequences to the larger scale circulation.

Results obtained represent an initial contribution in characterization and quantification of turbulent mixing in these important regions in the southwestern Atlantic Ocean and provide reference for future turbulence studies. Important conclusions regarding the dynamics of mixing in both areas were obtained, but more effort must be implemented to determine the variability of turbulent mixing dynamics in the SBS and the VTR.

As presented in this thesis, turbulence has important implications in the distribution of several properties in the ocean. Transports of momentum, heat, nutrients, chemicals and organisms are strongly related to the mixing pattern by turbulence and/or diffusion. Therefore, the knowledge of turbulence dynamics and its implications is very important in oceanographic research.

Bibliography

- Arruda, W. Z., Campos, E. J. D., Zharkov, V., Soutelino, R. G., and da Silveira, I. C. A. (2013). Events of equatorward translation of the Vitoria Eddy. *Continental Shelf Research*, 70:61–73.
- Borús, J., Uriburu Quirno, M., and Calvo, D. (2008). EVALUACIÓN DE CAUDALES DIARIOS DESCARGADOS POR LOS GRANDES RÍOS DEL SISTEMA DEL PLATA AL ESTUARIO DEL RÍO DE LA PLATA. *Dirección de Sistemas de Información y Alerta Hidrológico - Instituto Nacional del Agua - Ezeiza, Argentina*.
- Boussinesq, J. (1877). Essai sur la th?eorie des eaux courantes. *M?emoires pr?esent?es par divers savants a' l'Acad?emie des Sciences XXIII*, 1:1–680.
- Burrage, D., Wesson, J., Martinez, C., Pérez, T., Möller, O., and Piola, A. (2008). Patos Lagoon outflow within the Río de la Plata plume using an airborne salinity mapper: Observing an embedded plume. *Continental Shelf Research*, 28(13):1625–1638.
- Campos, P. C., Möller, O. O., Piola, A. R., and Palma, E. D. (2013). Seasonal variability and coastal upwelling near Cape Santa Marta (Brazil). *Journal of Geophysical Research: Oceans*, 118(3):1420–1433.
- Carter, G. S., Gregg, M. C., and Merrifield, M. A. (2006). Flow and Mixing around a Small Seamount on Kaena Ridge, Hawaii. *Journal of Physical Oceanography*, 36(6):1036–1052.
- Castello, J. P. and Möller, O. O. (1977). Sobre as condições oceanográficas do Rio Grande do Sul, Brasil. *Atlântica*, 1(2):25–110.
- Castro, B. M. (2014). Summer/winter stratification variability in the central part of the South Brazil Bight. *Continental Shelf Research*, 89:15–23.
- Cerda, C. and Castro, B. M. (2014). Hydrographic climatology of South Brazil Bight shelf waters between Sao Sebastiao (24°S) and Cabo Sao Tome (22°S). *Continental Shelf Research*, 89:5–14.
- Cushman-Roisin, B. and Beckers, J.-M. (2011). *Introduction to Geophysical Fluid Dynamics*. Academic Press.

- Da Silveira, I. C. A., Calado, L., Castro, B. M., Cirano, M., Lima, J. A. M., and Mascarenhas, A. d. S. (2004). On the baroclinic structure of the Brazil Current-Intermediate Western Boundary Current system at 22°-23°S. *Geophysical Research Letters*, 31(14):1–5.
- Da Silveira, I. C. A., Schmidt, A. C. K., Campos, E. D., de Godoi, S. S., and Ikeda, Y. (2000). A corrente do Brasil ao largo da costa leste brasileira. *Brazilian Journal of Oceanography*, 48(2):171–183.
- De Boyer Montégut, C., Madec, G., Fischer, A. S., Lazar, A., and Iudicone, D. (2004). Mixed layer depth over the global ocean: An examination of profile data and a profile-based climatology. *Journal of Geophysical Research C: Oceans*, 109(12):1–20.
- De Mesquita, A. R. and Harari, J. (2003). On the harmonic constants of tides and tidal currents of the South-eastern brazilian shelf. *Continental Shelf Research*, 23(11-13):1227–1237.
- De Ruitjer, W. P., Biastoch, A., Drijfhout, S., Lutjeharms, J. R. E., Matano, R., Pichevin, T., and Leeuwen, P. W. (1999). Indian-Atlantic interocean exchange: Dynamics, estimation and impact. *Journal of Geological Research*, 104.
- De Silva, I., Fernando, H., Eaton, F., and Hebert, D. (1996). Evolution of kelvin-helmholtz billows in nature and laboratory. *Earth and Planetary Science Letters*, 143(1):217 – 231.
- De Souza, R. B. and Robinson, I. S. (2004). Lagrangian and satellite observations of the Brazilian Coastal Current. *Continental Shelf Research*, 24(2):241–262.
- Decloedt, T. and Luther, D. S. (2010). On a Simple Empirical Parameterization of Topography-Catalyzed Diapycnal Mixing in the Abyssal Ocean. *Journal of Physical Oceanography*, 40(3):487–508.
- Dillon, T. M. (1982). Vertical overturns: A comparison of Thorpe and Ozmidov length scales. *Journal of Geophysical Research*, 87(C12):9601.
- Egbert, G. D. and Ray, R. D. (2000). Significant dissipation of tidal energy in the deep ocean inferred from satellite altimeter data. *Nature*, 405(6788):775–778.
- Fernández-Castro, B., Mouriño-Carballido, B., Benítez-Barrios, V. M., Chouciño, P., Fraile-Nuez, E., Graña, R., Piedeleu, M., and Rodríguez-Santana, A. (2014). Microstructure turbulence and diffusivity parameterization in the tropical and subtropical Atlantic, Pacific and Indian Oceans during the Malaspina 2010 expedition. *Deep-Sea Research Part I: Oceanographic Research Papers*, 94:15–30.

- Fong, D. A. and Geyer, W. R. (2001). Response of a river plume during an upwelling favorable wind event. *Journal of Geophysical Research*, 106:1067–1084.
- Gargett, A. (2003). Differential diffusion: an oceanographic primer. *Progress in Oceanography*, 56(3-4):559–570.
- Gargett, A. E. (1989). Ocean Turbulence. *Annual Review of Fluid Mechanics*, 21(1):419–451.
- Gargett, A. E. and Holloway, G. (1984). Dissipation and diffusion by internal wave breaking. *Journal of Marine Research*, 42(1):15–27.
- Gargett, A. E. and Moum, J. N. (1995). Mixing Efficiencies in Turbulent Tidal Fronts: Results from Direct and Indirect Measurements of Density Flux. *Journal of Physical Oceanography*, 25(11):2583–2608.
- Garrett, C. and Kunze, E. (2007). Internal Tide Generation in the Deep Ocean. *Annual Review of Fluid Mechanics*, 39(1):57–87.
- Gibson, C. H. and Schwarz, W. H. (1963). The universal equilibrium spectra of turbulent velocity and scalar fields. *Journal of Fluid Mechanics*, 16:365–384.
- Goni, G. J. and Wainer, I. (2001). Investigation of the Brazil Current front variability from altimeter data. *Journal of Geophysical Research*, 106(C12):31117.
- Grant, H. L., Stewart, R. W., and Moilliet, A. (1962). Turbulence spectra from a tidal channel. *Journal of Fluid Mechanics*, 12(2):241–268.
- Gregg, M. C. (1977). Variations in the Intensity of Small-Scale Mixing in the Main Thermocline. *Journal of Physical Oceanography*, 7(3):436–454.
- Gregg, M. C. (1989). Scaling turbulent dissipation in the thermocline. *Journal of Geophysical Research*, 94(C7):9686–9698.
- Gregg, M. C. (1999). Uncertainties and limitations in measuring ϵ and $\chi(T)$. *Journal of Atmospheric and Oceanic Technology*, 16(11 PART 1):1483–1490.
- Gregg, M. C. and Meagher, T. B. (1980). The dynamic response of glass rod thermistors. *Journal of Geophysical Research*, 85(C5):2779–2786.
- Guerrero, R., Acha, E. M., Framián, M. B., and Lasta, C. A. (1997). Physical oceanography of the Rio de la Plata Estuary, Argentina. *Continental Shelf Research*, 17(7):727–742.

- Hall, R. a., Huthnance, J. M., and Williams, R. G. (2013). Internal Wave Reflection on Shelf Slopes with Depth-Varying Stratification. *Journal of Physical Oceanography*, 43(2):248–258.
- Hetland, R. D. (2005). Relating River Plume Structure to Vertical Mixing. *Journal of Physical Oceanography*, 35(9):1667–1688.
- Horner-Devine, A. R., Hetland, R. D., and MacDonald, D. G. (2015). Mixing and Transport in Coastal River Plumes. *Annu. Rev. Fluid Mech.*, 47(1):569–594.
- Ivey, G., Winters, K., and Koseff, J. (2008). Density stratification, turbulence, but how much mixing? *Annual Review of Fluid Mechanics*, 40(1):169–184.
- Ivey, G. N. and Imberger, J. (1991). On the Nature of Turbulence in a Stratified Fluid. Part I: The Energetics of Mixing. *Journal of Physical Oceanography*, 21(5):650–658.
- Ivey, G. N. and Nokes, R. I. (1989). Vertical mixing due to the breaking of critical internal waves on sloping boundaries. *Journal of Fluid Mechanics*, 204:479–500.
- Johnston, T. M. S. (2003). Internal tide scattering at seamounts, ridges, and islands. *Journal of Geophysical Research*, 108(C6):3180.
- Kelley, D. E., Fernando, H. J., Gargett, A. E., Tanny, J., and Özsoy, E. (2003). The diffusive regime of double-diffusive convection. *Progress in Oceanography*, 56(3-4):461–481.
- Klymak, J. M., Moum, J. N., Nash, J. D., Kunze, E., Girton, J. B., Carter, G. S., Lee, C. M., Sanford, T. B., and Gregg, M. C. (2006). An Estimate of Tidal Energy Lost to Turbulence at the Hawaiian Ridge. *Journal of Physical Oceanography*, 36(6):1148–1164.
- Kolmogorov, A. N. (1968). Local structure of turbulence in an incompressible viscous fluid at very large reynolds numbers. *Soviet Physic. Uspekhi*, 10(6):476–481.
- Kundu, P. K., Cohen, I. M., and Dowling, D. R. (2001). *Fluid Mechanics*. Academic Press, 5th edition.
- Kunze, E. (1994). A proposed flux constraint for salt fingers in shear. *Journal of Marine Research*, 52(6):999–1016.
- Kunze, E. (2003). A review of oceanic salt-fingering theory. *Progress in Oceanography*, 56(3-4):399–417.
- Kunze, E., Firing, E., Hummon, J. M., Chereskin, T. K., and Thurnherr, A. M. (2006). Global Abyssal Mixing Inferred from Lowered ADCP Shear and CTD Strain Profiles. *Journal of Physical Oceanography*, 36(8):1553–1576.

- Kunze, E. and Sanford, T. B. (1996). Abyssal Mixing: Where It Is Not. *Journal of Physical Oceanography*, 26(10):2286–2296.
- Lamb, K. G. (2014). Internal Wave Breaking and Dissipation Mechanisms on the Continental Slope/Shelf. *Annual Review of Fluid Mechanics*, 46(1):231–254.
- Ledwell, J. R., Watson, A. J., and Law, C. S. (1993). Evidence for slow mixing across the pycnocline from an open-ocean tracer-release experiment. *Nature*, 364(6439):701–703.
- Legg, S. (2016). Internal Tide Breaking at Topography. In *20th Australasian Fluid Mechanics Conference*, volume 1.
- Lentz, S. (2004). The Response of Buoyant Coastal Plumes to Upwelling-Favorable Winds. *Journal of Physical Oceanography*, 34(11):2458–2469.
- Lien, R. C. and Gregg, M. C. (2001). Observations of turbulence in a tidal beam and across a coastal ridge. *Journal of Geophysical Research*, 106(C3):4575.
- Lima, I. D., Garcia, C. A. E., and Möller, O. O. (1996). Ocean surface processes on the Southern Brazilian shelf: Characterization and seasonal variability. *Continental Shelf Research*, 16(10):1307–1317.
- Lowe, R. J., Rottman, J. W., and Linden, P. F. (2005). The non-Boussinesq lock-exchange problem. Part 1. Theory and experiments. *Journal of Fluid Mechanics*, 537:101–124.
- Lueck, R. G. and Mudge, T. (1997). Topographically Induced Mixing Around a Shallow Seamount. *Science*, 276(5320):1831–1833.
- Lueck, R. G., Wolk, F., and Yamazaki, H. (2002). Oceanic velocity microstructure measurements in the 20th century. *Journal of Oceanography*, 58(1):153–174.
- Luketina, D. A. and Imberger, J. (1989). Turbulence and entrainment in a buoyant surface plume. *Journal of Geophysical Research: Oceans*, 94(C9):12619–12636.
- MacDonald, D. G., Carlson, J., and Goodman, L. (2013). On the heterogeneity of stratified-shear turbulence: Observations from a near-field river plume. *Journal of Geophysical Research: Oceans*, 118(11):6223–6237.
- MacDonald, D. G., Goodman, L., and Hetland, R. D. (2007). Turbulent dissipation in a near-field river plume: A comparison of control volume and microstructure observations with a numerical model. *Journal of Geophysical Research: Oceans*, 112(7):1–13.

- Marcelo Acha, E., Mianzan, H., Guerrero, R., Carreto, J., Giberto, D., Montoya, N., and Carignan, M. (2008). An overview of physical and ecological processes in the Rio de la Plata Estuary. *Continental Shelf Research*, 28(13):1579–1588.
- Matano, R. P., Palma, E. D., and Piola, A. R. (2010). The influence of the Brazil and Malvinas Currents on the Southwestern Atlantic Shelf circulation. *Ocean Science*, 6(4):983–995.
- Mater, B. D., Schaad, S. M., and Venayagamoorthy, S. K. (2013). Relevance of the Thorpe length scale in stably stratified turbulence. *Physics of Fluids*, 25(7).
- McWilliams, J. C., Sullivan, P. P., and Moeng, C.-H. (1997). Langmuir turbulence in the ocean. *Journal of Fluid Mechanics*, 334(April):1–30.
- Merryfield, W. J., Holloway, G., and Gargett, A. E. (1998). Differential vertical transport of heat and salt by weak stratified turbulence. *Geophysical Research Letters*, 25(15):2773–2776.
- Moller, O. O., Castaing, P., Salomon, J.-C., and Lazure, P. (2001). The Influence of Local and Non-Local Forcing Effects on the Subtidal Circulation of Patos Lagoon. *Estuaries*, 24(2):297.
- Möller, O. O., Piola, A. R., Freitas, A. C., and Campos, E. J. D. (2008). The effects of river discharge and seasonal winds on the shelf off southeastern South America. *Continental Shelf Research*, 28(13):1607–1624.
- Moraes, O. L., Degrazia, G. A., and Tirabassi, T. (1998). Using the Prandtl-Kolmogorov relationship and spectral modeling to derive an expression for the eddy diffusivity coefficient for the stable boundary layer. *Nuovo Cimento della Societa Italiana di Fisica D - Condensed Matter, Atomic, Molecular and Chemical Physics, Biophysics*, 20(6):791–798.
- Motoki, A., Motoki, K. F., and Melo, D. P. D. (2012). Caracterização da morfologia submarina da cadeia Vitória-Trindade e áreas adjacentes-ES, com base na batimetria predita do topo versão 14.1. *Revista Brasileira de Geomorfologia*, 13(2):151–170.
- Moum, J. N. (1996). Efficiency of mixing in the main thermocline. *Journal of Geophysical Research: Oceans*, 101(C5):12177–12191.
- Moum, J. N. and Rippeth, T. P. (2009). Do observations adequately resolve the natural variability of oceanic turbulence? *Journal of Marine Systems*, 77(4):409–417.
- Munk, W. and Wunsch, C. (1986). Abyssal recipes II: energetics of tidal and wind mixing. *Deep-Sea Research I*, 45:1977–2010.

- Nash, J. D. and Moum, J. N. (1999). Estimating salinity variance dissipation rate from conductivity microstructure measurements. *Journal of Atmospheric and Oceanic Technology*, 16(2):263–274.
- Nash, J. D. and Moum, J. N. (2001). Internal hydraulic flows on the continental shelf: High drag states over a small bank. *Journal of Geophysical Research-Oceans*, 106(C3):4593–4611.
- Nasmyth, P. W. (1970). *Ocean turbulence*. PhD thesis, Department of Physics, University of British Columbia.
- Oakey, N. S. (1982). Determination of the Rate of Dissipation of Turbulent Energy from Simultaneous Temperature and Velocity Shear Microstructure Measurements. *Journal of Physical Oceanography*, 12:256–271.
- O'Donnell, J., Ackleson, S. G., and Levine, E. R. (2008). On the spatial scales of a river plume. *Journal of Geophysical Research: Oceans*, 113(4):1–12.
- Olson, D. B., Podestá, G. P., Evans, R. H., and Brown, O. B. (1988). Temporal variations in the separation of Brazil and Malvinas Currents. *Deep Sea Res. Part A, Oceanogr. Res. Pap.*, 35(12):1971–1990.
- Osborn, T. R. (1974). Vertical Profiling of Velocity Microstructure. *Journal of Physical Oceanography*, 4(1):109–115.
- Osborn, T. R. (1980). Estimates of the Local Rate of Vertical Diffusion from Dissipation Measurements. *Journal of Physical Oceanography*, 10(1):83–89.
- Osborn, T. R. and Cox, C. S. (1972). Oceanic fine structure. *Geophysical Fluid Dynamics*, 3(1):321–345.
- Padman, L. (1994). Momentum fluxes through sheared oceanic thermohaline steps. *Journal of Geophysical Research: Oceans*, 99:491–513.
- Pereira, A. F., Belém, A. L., Castro, B. M., and Geremias, R. (2005). Tide-topography interaction along the eastern Brazilian shelf. *Continental Shelf Research*, 25(12-13):1521–1539.
- Peters, H. (1997). Observations of Stratified Turbulent Mixing in an Estuary: Neap-to-spring Variations During High River Flow. *Estuarine, Coastal and Shelf Science*, 45:69–88.
- Peterson, R. G. and Stramma, L. (1991). Upper-level circulation in the South-Atlantic Ocean. *Progress In Oceanography*, 26(1):1–73.

- Pimenta, F. M., Campos, E. J. D., Miller, J. L., and Piola, A. R. (2005). A numerical study of the Plata River plume along the southeastern South American continental shelf. *Brazilian Journal of Oceanography*, 53(869):129–146.
- Pineiro, H. T., Mazzei, E., Moura, R. L., Amado-Filho, G. M., Carvalho-Filho, A., Braga, A. C., Costa, P. A. S., Ferreira, B. P., Ferreira, C. E. L., Floeter, S. R., Francini-Filho, R. B., Gasparini, J. L., Macieira, R. M., Martins, A. S., Olavo, G., Pimentel, C. R., Rocha, L. A., Sazima, I., Simon, T., Teixeira, J. B., Xavier, L. B., and Joyeux, J. C. (2015). Fish biodiversity of the Vitória-Trindade seamount chain, southwestern Atlantic: An updated database. *PLoS ONE*, 10(3):1–17.
- Piola, A., Campos, E., and Jr, O. M. (1999). Continental shelf water masses off eastern South America 20 to 40 S. *Symposium On Global . . .*
- Price, J. F. and Weller, R. A. (1986). Diurnal Cycling: Observation and models of the upper ocean response to diurnal heating, cooling and wind mixing. *Journal of Geophysical Research*, 91:8411–8427.
- Ribner, H. S. and Siddon, T. E. (1965). An aerofoil probe for measuring the transverse component of turbulence. *AIAA Journal*, 3(4):747–749.
- Riser, S. and Owens, W. (1986). The structure, dynamics, and origin of a small-scale lens of water in the western North Atlantic thermocline. *Journal of Physical Oceanography*, 16(3):572–590.
- Robertson, A. W. and Mechoso, C. R. (1998). Interannual and decadal cycles in river flows of southeastern south america. *Journal of Climate*, 11(10):2570–2581.
- Rudnick, D. L. and Klinke, J. (2007). The underway conductivity-temperature-depth instrument. *Journal of Atmospheric and Oceanic Technology*, 24(11):1910–1923.
- Salmon, R. (1998). *Lectures on geophysical fluid dynamics*. Oxford University Press, New York. n/a.
- Sarkar, S. and Scotti, A. (2017). From Topographic Internal Gravity Waves to Turbulence. *Annual Review of Fluid Mechanics*, 49(1):195–220.
- Schmid, C., Schäfer, H., Zenk, W., and Podestá, G. (1995). The Vitória Eddy and Its Relation to the Brazil Current. *Journal Physical Oceanography*, 25(11):2532–2546.
- Schmitt, R. W. (1979). The growth rate of super-critical salt fingers. *Deep Sea Research Part A. Oceanographic Research Papers*, 26(1):23–40.

- Schmitt, R. W. (1981). Form of the temperature-salinity relationship in the central water: Evidence for double-diffusive mixing. *Journal of Physical Oceanography*, 11(7):1015–1026.
- Schmitt, R. W. (1994). Double Diffusion in Oceanography. *Annual Review of Fluid Mechanics*, 26(1):255–285.
- Schmitt, R. W. (2003). Observational and laboratory insights into salt-finger convection. *Progress in Oceanography*, 56(3-4):10.
- Schmitt, R. W. and Evans, D. L. (1978). An estimate of the vertical mixing due to salt fingers based on observations in the north atlantic central water. *Journal of Geophysical Research: Oceans*, 83(C6):2913–2919.
- Shay, T. J. and Gregg, M. C. (1986). Convectively Driven Turbulent Mixing in the Upper Ocean. *Journal of Geophysical Research*, 16(11):1777–1798.
- Simpson, J. and Sharples, J. (2012). *Introduction to the physical and biological oceanography of shelf seas*. Cambridge University Press.
- Simpson, J. H. (1997). Physical processes in the ROFI regime. *Journal of Marine Systems*, 12(1-4):3–15.
- Simpson, J. H., Hyder, P., Rippeth, T. P., and Lucas, I. M. (2002). Forced Oscillations near the Critical Latitude for Diurnal-Inertial Resonance. *Journal of Physical Oceanography*, 32(1):177–187.
- Sinha, N. (2013). *Towards RANS Parameterization of Vertical Mixing by Langmuir Turbulence in Shallow Coastal Shelves*. PhD thesis, Civil and Environmental Engineering, University of South Florida.
- Smyth, W. D. and Moum, J. N. (2000). Length scales of turbulence in stably stratified mixing layers. *Phys. Fluids*, 12(6):1327.
- Smyth, W. D., Moum, J. N., and Caldwell, D. R. (2001). The Efficiency of Mixing in Turbulent Patches: Inferences from Direct Simulations and Microstructure Observations. *Journal of Physical Oceanography*, 31(8):1969–1992.
- Soares, I. and Möller, O. (2001). Low-frequency currents and water mass spatial distribution on the southern Brazilian shelf. *Continental Shelf Research*, 21(16-17):1785–1814.
- Soutelino, R. G., Da Silveira, I. C. A., Gangopadhyay, A., and Miranda, J. A. (2011). Is the Brazil Current eddy-dominated to the north of 20S. *Geophysical Research Letters*, 38(3):1–5.

- Soutelino, R. G., Gangopadhyay, A., and Da Silveira, I. C. A. (2013). The roles of vertical shear and topography on the eddy formation near the site of origin of the Brazil Current. *Continental Shelf Research*, 70:46–60.
- Souza, A. J., Burchard, H., Eden, C., Pattiaratchi, C., and Van Haren, H. (1997). Coastal Ocean Turbulence and Mixing. *Coupled Coastal Wind, Wave and Current Dynamics*.
- St. Laurent, L. and Schmitt, R. W. (1999). The Contribution of Salt Fingers to Vertical Mixing in the North Atlantic Tracer Release Experiment*. *J. Phys. Oceanogr.*, 29(7):1404–1424.
- Stacey, M. T., Monismith, S. G., and Burau, J. R. (1999). Observations of Turbulence in a Partially Stratified Estuary. *Journal of Physical Oceanography*, 29(8):1950–1970.
- Stech, J. L. and Lorenzetti, J. A. (1992). The Response of the south Brazil bight to the passagem of wintertime cold fronts. *Journal of Geophysical Research*, 97(C6):9507–9520.
- Steinbuck, J. V., Stacey, M. T., and Monismith, S. G. (2009). An evaluation of χ^2 estimation techniques: Implications for Batchelor fitting and ϵ . *Journal of Atmospheric and Oceanic Technology*, 26(8):1652–1662.
- Stern, M. E. (1960). The Salt-Fountain and Thermohaline Convection. *Tellus*, 12(2):172–175.
- Stramma, L. and England, M. (1999). On the water masses and mean circulation of the South Atlantic Ocean. *Journal of Geophysical Research: Oceans*, 104(C9):20863–20883.
- Tennekes, H. and Lumley, J. (1972). *A first course in turbulence*. M.I.T. Press.
- Thomson, R. E. and Fine, I. V. (2003). Estimating mixed layer depth from oceanic profile data. *Journal of Atmospheric and Oceanic Technology*, 20(2):319–329.
- Thorpe, S. A. (2004). Recent Developments in the Study of Ocean Turbulence. *Annual Reviews in Earth and Planetary Sciences*, 32(1):91–109.
- Thorpe, S. A. (2007). *An Introduction to Ocean Turbulence*. Cambridge University Press.
- Toole, J. M., Schmitt, R. W., Polzin, K. L., and Kunze, E. (1997). Near-boundary mixing above the flanks of a midlatitude seamount. *Journal of Geophysical Research: Oceans*, 102(96):947–959.

- Turner, J. S. (1968). The influence of molecular diffusivity on turbulent entrainment across a density interface. *Journal of Fluid Mechanics*, 33(4):639–656.
- Wain, D. J., Lilly, J. M., Callaghan, A. H., Yashayaev, I., and Ward, B. (2015). A breaking internal wave in the surface ocean boundary layer. *Journal of Geophysical Research C: Oceans*, 120(6):4151–4161.
- Wang, D. (1984). Mutual intrusion of a gravity current and density front formation. *Journal of Physical Oceanography*, 14(7):1191–1199.
- Wang, J., MacDonald, D. G., Orton, P. M., Cole, K., and Lan, J. (2015). The Effect of Discharge, Tides, and Wind on Lift-Off Turbulence. *Estuaries and Coasts*, 38(6):2117–2131.
- Wunsch, C. (1968). On the propagation of internal waves up a slope. *Deep-Sea Research*, 15(2070):251–258.
- Yankovsky, A. E. (2006). On the validity of thermal wind balance in alongshelf currents off the New Jersey coast. *Continental Shelf Research*, 26(10):1171–1183.
- Zavialov, P., Möller, O., and Campos, E. (2002). First direct measurements of currents on the continental shelf of Southern Brazil. *Continental Shelf Research*, 22(14):1975–1986.
- Zavialov, P. and Möller, O. O. (1998). Modeling and observations of currents off southern Brazil and Uruguay: the Rio Grande Current. In *Proceedings of Oceanic Fronts and Related Problems: Kostantin Fedorov International Memorial Symposium, Saint Petersburg, Russia*, number 159, pages 612–617.